

Structural Integrity Study Concerning LTCP Phenomenon

Author: Otso Cronvall

Confidentiality: Public




Report's title Structural Integrity Study Concerning LTCP Phenomenon	
Customer or financing body and order date/No. VTT, VYR	Order reference ad 23/2007SAF
Project name SAFIR2010/DEFSPEED	Project number/Short name 41755/DEFSPEED
Author Otso Cronvall	Pages 42/-
Keywords LTCP, DMW, safe-end, J -integral, VTTBESIT, DIFF	Research report No. VTT-R-00055-11
<p>Summary</p> <p>This study concerns structural integrity analyses in connection with low temperature crack propagation (LTCP) phenomenon. The LTCP is associated with relatively low material fracture toughness values. Especially this phenomenon concerns pressurised water reactor (PWR) plants because, and unlike boiling water reactor (BWR) plants, PWR environments contain a notable amount of hydrogen.</p> <p>In this study the structural integrity analyses were performed to a dissimilar metal weld (DMW) at a nozzle/safe-end joint resembling that in PWR plants. To assess how the LTCP could effect in a more severe case, the considered material was Alloy 182, as in relation to the LTCP it is associated with markedly low fracture toughness. Here the needed fracture toughness data was obtained from the recent VTT experiments [1]. First step in the structural integrity analyses was to compute the transient heat transfer and stress/strain distributions through the DMW wall. Weld residual stress (WRS) distributions were also taken into account, here according to handbook assumptions. Then the crack sensitivity analyses were performed using both analytical equations and a fracture mechanics based analysis code VTTBESIT, developed both at VTT and IWM [18, 19, 20]. In the crack sensitivity analyses the considered crack postulate was an axial half-elliptic crack in the inner surface of the assumed DMW at a nozzle/safe-end joint, with covering a representative set of aspect ratios, while two load cases were considered. The considered limiting criterion in the present analyses is crack tip value of mode I J-integral, J_I, reaching the corresponding fracture toughness, J_{IC}.</p> <p>For analysis cases exceeding the experimentally defined J_{IC} values associated with the LTCP, the corresponding crack sizes are relatively large, e.g. in the depth direction from 52 to 98 % of the wall thickness, which was assumed as 40 mm. Growing cracks are most likely detected in the inspections with non-destructive testing (NDT) techniques before they reach these large sizes. On the other hand, if J_I values of a crack reach the corresponding J_{IC} value under LTCP conditions, the resulting crack growth could be fast and lead to a leaking crack before the next inspections. According to present analysis results for narrow cracks with aspect ratio of 1/1 the J_I values stay below the considered J_{IC} values.</p> <p>Some suggestions for possible further research were identified. These concern both experimental research and further development of simulation/computation approaches.</p>	
Date Espoo, 17 January 2011	
Written by	Reviewed by
	
Accepted by	
	
Otso Cronvall Research Scientist	Heikki Keinänen Senior Research Scientist
	Eila Lehmus Technology Manager
Kemistintie 3, Espoo P.O. Box 1000 FI-02044 VTT, Finland	
Distribution (customer and VTT): VTT, SAFIR2010 TR6, Karen Gott, SSM, YVL data base	
<i>The use of the name of the VTT Technical Research Centre of Finland (VTT) in advertising or publication in part of this report is only permissible with written authorisation from the VTT Technical Research Centre of Finland.</i>	

Table of contents

Abbreviations and symbols	3
1 Introduction	5
2 Geometry and crack postulate data	7
3 Material properties	8
4 Loads	10
4.1 Loads considered in the analyses	10
4.2 Transient load cases	11
4.3 Welding process induced residual stresses	14
5 Heat transfer and stress analyses	17
5.1 Overview of performed heat transfer and stress analyses	17
5.2 Applied analytical stress computation equations	17
5.3 Analysis code DIFF	18
5.4 Summary of heat transfer and stress analysis results	18
6 Crack sensitivity analyses and their results	27
6.1 Analysed crack postulates and associated input data	27
6.2 Limiting crack sizes	28
6.3 Steps of performed crack sensitivity analyses.....	28
6.4 Computer code used in fracture mechanics analyses.....	30
6.5 Results from crack sensitivity analyses	31
7 Summary and conclusions	38
References	41

Abbreviations and symbols

Abbreviations

ASME	American Society of Mechanical Engineers
BWR	Boiling water reactor
DMW	Dissimilar metal weld
ECC	Emergency core cooling
FEM	Finite element method
HAZ	Heat affected zone
LOCA	Loss-of-coolant-accident
LTCP	Low temperature crack propagation
NPP	Nuclear power plant
PWHT	Post-weld heat treatment
PWR	Pressurised water reactor
RPV	Reactor pressure vessel
SCC	Stress corrosion cracking
WRS	Weld residual stress

Latin letters

a	Crack depth [mm]
a_{eff}	effective crack depth [mm]
c	Half of crack length [mm]
c	Specific heat [J/kg°C]
E	Elastic modulus, Young's modulus [N/mm ²]
t_w	Wall thickness [mm]
J_{el}	Elastic J -integral [kJ/m ²]
J_{ep}	Elastic-plastic J -integral [kJ/m ²]
J_{IC}	Mode I fracture toughness in terms of J -integral [kJ/m ²]
J_{pl}	Plastic J -integral [kJ/m ²]
K_I	Stress intensity factor, mode I [MPa√m]
K_{Ip}	Plasticity corrected mode I stress intensity factor [MPa√m]
l	Crack length [mm]
p	Pressure [N/mm ²]
P	Inner pressure corresponding to prevailing loads [MPa]
P_L	Limit load [MPa]
r	Radial coordinate through wall [mm]
R	Mean radius [mm]
R_i	Inner pipe cross-section radius [mm]
R_o	Outer pipe cross-section radius [mm]
S_m	Design stress [N/mm ²]
S_r	Material yield stress at the considered temperature acc. to SSM handbook [N/mm ²]
S_u	Tensile Strength [N/mm ²]
S_y	Yield Strength [N/mm ²]

t	Time [s]
t	Wall thickness of pipe cross-section acc. to SSM handbook [mm]
t_w	Wall thickness of pipe cross-section [mm]
T	Temperature [°C]
u	Radial coordinate through pipe wall with origin at inner surface of the pipe acc. to SSM handbook [mm]

Greek letters

α_T	Coefficient of thermal expansion [1/°C]
β, μ	Equation coefficients to take into account plane stress or plain strain conditions [-]
ε_{ref}	Reference strain [mm/mm]
ϕ	Angular position in the front of a half-elliptical surface crack, the origin of which is in the axis parallel to crack postulate length [°]
λ	Thermal conductivity [W/m°C]
ν	Poisson's coefficient [-]
ρ	Density [kg/m ³]
σ	Weld residual stress across the wall thickness acc. to SSM handbook [N/mm ²]
$\sigma_{AXIAL,p}$	Longitudinal/axial stress caused by pressure [N/mm ²]
$\sigma_{CIRC,p}$	Longitudinal/axial stress caused by pressure [N/mm ²]

1 Introduction

This study concerns structural integrity analyses in connection with low temperature crack propagation (LTCP) phenomenon. The LTCP is associated with decreased fracture toughness values as compared to those in air. Especially this phenomenon concerns pressurised water reactor (PWR) plants because, and unlike boiling water reactor (BWR) plants, PWR environments contain a notable amount of hydrogen.

In this study the structural integrity analyses were performed to a dissimilar metal weld (DMW) at a nozzle/safe-end joint resembling that in PWR plants. The considered material was Alloy 182, as in relation to the LTCP it is associated with low fracture toughness. Here the needed fracture toughness data were obtained from the recent VTT experiments, as reported in ref. [1]. Important associated background research work is presented in the quite recent Master's Thesis [2]. The first step in the structural integrity analyses was to compute the transient heat transfer and stress/strain distributions through the DMW wall. This was carried out using analytical equations and numerical temperature/stress analysis code DIFF developed at VTT [10]. Also weld residual stress (WRS) distributions were taken into account, here according to assumptions in the SSM Handbook [17]. Then the crack sensitivity analyses were performed using both analytical equations and a fracture mechanics based analysis code VTTBESIT, developed both at VTT and IWM [18, 19, 20]. In the crack sensitivity analyses the considered crack postulate was axial half-elliptic crack in the inner surface of the assumed DMW at a nozzle/safe-end joint, with covering a representative set of aspect ratios, while the considered load cases were Shutdown and Emergency cooling transients. As the considered material is an austenitic alloy with relatively large strain hardening region, elastic-plastic fracture mechanics procedures associated with assessment of ductile fracture were applied. As for the considered limiting criterion, in the present analyses it was the crack tip value of J -integral reaching the corresponding fracture toughness, J_{IC} .

As for the above mentioned VTT experiments [1], the effect of hydrogenated PWR primary water on the LTCP susceptibility of nickel based weld metals Alloy 182, 82, 152 and 52 was studied performing J - R tests at a slow displacement rate in low temperature hydrogenated water. When tested in an environment with high hydrogen content ($100 \text{ cm}^3 \text{ H}_2/\text{kg H}_2\text{O}$), all the studied materials showed a remarkable decrease in the fracture toughness (J_{IC} or J_Q) values compared with the air test results. Alloy 182 showed the lowest average fracture toughness values in each test environment. The results obtained at lower hydrogen content ($\sim 30 \text{ cm}^3 \text{ H}_2/\text{kg H}_2\text{O}$) suggest, that Alloy 182 is the most susceptible nickel based weld metal to LTCP. Intergranular cracking mode was predominant when the J_{IC} value was low. Test results of pure weld metal Alloys 182 and 52 were also compared with the results of DMW specimens of Alloy 182 and 52. The pure weld metals were substantially more susceptible to LTCP than the DMW specimens. Pre-exposure to high temperature hydrogenated water did not affect the fracture toughness of any of the test materials. The degradation in toughness is assumed to be caused by hydrogen induced intergranular cracking mechanism.

The geometry of the assumed DMW joint and crack postulates are presented in Chapter 2. Then, the material properties and loads of the examined components are presented in Chapters 3 and 4, respectively. The heat transfer and stress analyses of the examined component are presented in Chapter 5. The characteristics and summary of the results of the performed crack sensitivity

analyses are presented in Chapter 6. The report ends with a summary, conclusions and some suggestions for further research, presented in Chapter 7.

2 Geometry and crack postulate data

In this study the structural integrity analyses were performed to a DMW at a nozzle/safe-end joint resembling that in PWR plants. The overall geometry of the assumed DMW joint together with the considered crack postulate are shown in the Figure 2-1 below. Here the symmetry axis of the crack postulate coincides with weld centre-line, because most often WRSs, being the dominant stress component within the weld region, are assumed to reach their maximum values in the middle of weld. From the viewpoint of a possible pipe break a circumferentially oriented crack postulate would be more threatening. However, for nozzle/safe-end joint welds axially oriented cracks are more likely, also circumferential stresses causing the growth of such cracks are considerably higher than the corresponding axial stresses propagating circumferential cracks.

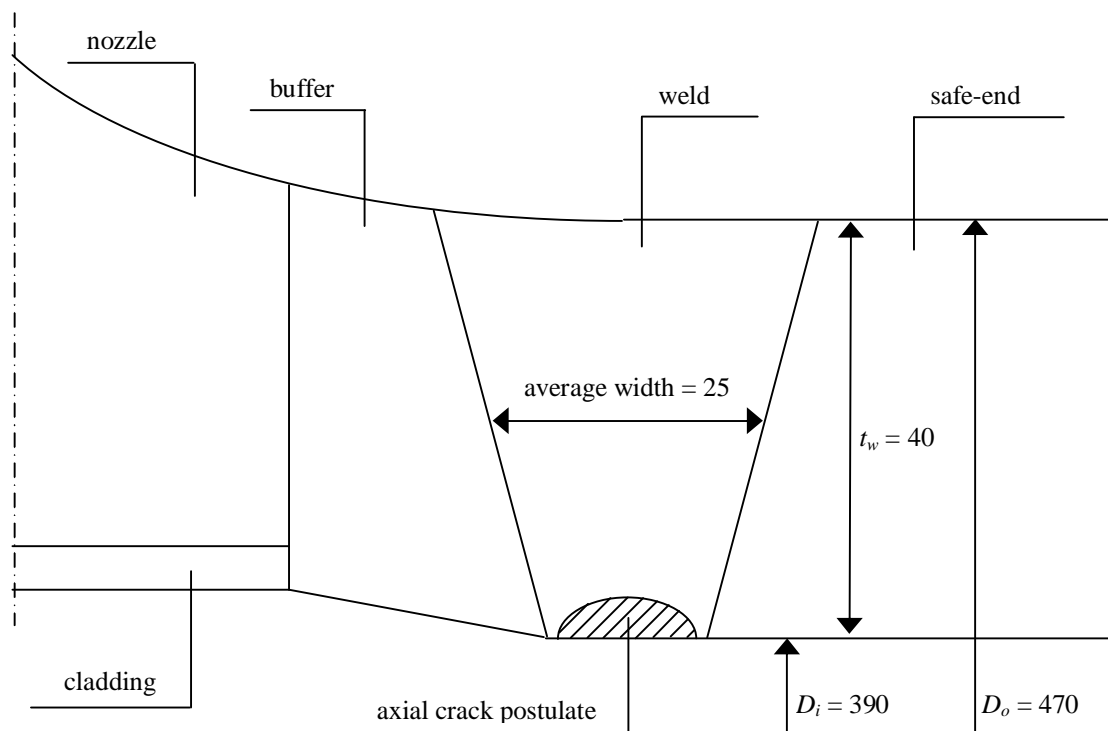


Figure 2-1. The overall geometry of the examined DMW joint together with some assumed dimensions and the considered crack postulate. Concerning notations; t_w [mm] is wall thickness, D_i [mm] is inner diameter and D_o [mm] is outer diameter.

The materials of the assumed DMW joint and connecting components are as follows:

- weld and buffer; Alloy 182,
- safe-end and cladding; austenitic material,
- nozzle; ferritic steel.

In the present crack sensitivity analyses the following crack postulates were considered:

- main characteristics; axial half-elliptical crack in the inner surface of the assumed DMW with the centre-line coinciding with that of the weld,
- considered aspect ratios; 1/1, 1/3, 1/5 and 1/10.

3 Material properties

The following material properties are presented here in Tables 3-1 to 3-3 for the considered Alloy 182: yield strength, design stress, tensile strength, elastic modulus, thermal conductivity, specific heat, coefficient of thermal expansion, Poisson’s coefficient and density. All of the above mentioned material properties are presented as a function of temperature within the range of 20 °C to 300 °C besides Poisson’s coefficient and density, since their dependency of temperature in this temperature range is negligible.

All of the material properties presented in the following tables are considered typical. They are neither average nor minimum. Thermal–physical properties such as thermal expansion, thermal conductivity, and thermal diffusivity are affected more by alloy content than by crystal structure or heat treatment. Due to the permitted range for elements comprising alloys (specification ranges of chemical compositions), the thermal–physical properties should be considered to have an associated uncertainty of ±10%. Values of specific heat should also be assumed to have the same associated ±10% uncertainty. Modules of elasticity and rigidity as well as Poisson’s ratio are also typical values, but the values of modulus of elasticity, given as a function of temperature, tend to be closer to average values since their temperature dependency is factored against an “average” room temperature value [13]. In the analyses linear interpolation was performed for the material property values falling between those presented here.

It is assumed here that the DMW region of the joint structure has not been in post weld heat treatment (PWHT), which is quite common for safe-end/nozzle DMWs.

Table 3-1. Strength properties used for Alloy 182 as a function of temperature see Tables 2a, U and Y-1 in Section II of ASME code [13].

Temperature T [°C]	Yield strength S_y [N/mm ²]	Design stress S_m [N/mm ²]	Tensile strength S_u [N/mm ²]
21	241	137	586
93	229	137	586
149	223	137	586
204	220	137	586
260	220	137	586
286	220	137	586
316	220	137	586

Table 3-2. Some mechanical properties used for Alloy 182 as a function of temperature, see Tables TCD, TE-1 and TM-1 of Part D of Section II of ASME code [13].

Temperature T [°C]	Elastic modulus E [GPa]	Thermal conductivity λ [W/m°C]	Specific heat c [J/kg°C]	Coefficient of thermal expansion $\alpha_T \cdot 10^{-06}$ [1/°C]
21	213.7	14.9	451	12.2
38		15.1	456	12.4
66		15.4	464	12.7
93	208.2	15.8	471	13.0
121		16.1	475	13.2
149	206.2	16.6	485	13.3
177		17.0	486	13.5
204	203.4	17.5	494	13.6
232		17.8	495	13.8
260	199.9	18.3	501	13.9
288		18.7	507	14.0
316	197.9	19.2	515	14.1

Table 3-3. Values of density and Poisson's coefficient for Alloy 182, see ref. [13].

Density ρ [kg/m ³]	Poisson's coefficient ν [-]
7850	0.3

The fracture toughness data concerning Alloy 182, as presented in Table 3-4 in the following, were obtained from the recent VTT experiments [1]. These experiments consisted of hydrogenated PWR water tests with two levels of hydrogen content, those being 33 cm³ H₂/kg H₂O and 100 cm³ H₂/kg H₂O, and for the latter hydrogen content also one set of tests with pre-exposure of 24 h at 300 °C. For all these experiments the temperature was kept at constant value of 55 °C.

Table 3-4. The fracture toughness data concerning Alloy 182 from the recent VTT experiments, as reported in ref. [1].

Hydrogen content	Pre-exposure	average J_{IC} [kJ/m ²]
33 cm ³ H ₂ /kg H ₂ O	None	81
100 cm ³ H ₂ /kg H ₂ O	24 h at 300 °C	41
100 cm ³ H ₂ /kg H ₂ O	None	64

4 Loads

4.1 Loads considered in the analyses

In general the stresses and strains acting in DMWs at PWR nozzle/safe-end joints are caused by various load cases and types of loads. However, most of the time PWR plants are under quasi-static operational conditions, with constant values for pressure and temperature, those being e.g. for OL3 NPP primary circuit 155 bar with 296 °C for cold leg and 329 °C for hot leg [3], respectively. In the following Table 4-1 are presented typical operational temperatures and pressures for common PWR plant types.

Table 4-1. Typical operational temperatures for common PWR plant types [4].

Parameter/Reactor type	Westinghouse (4-loop plant)	Framatome	Siemens	WWER 440	WWER 1000	EPR
Cold leg temperature, °C	292.5	292	291.3	270	290	295.5
Hot leg temperature, °C	325.5	329.5	326.1	300	325	328
Primary circuit pressure, MPa	15.51	15.51	15.2-15.8	12.2-12.5	15.7	15.5

The deviations from the operational conditions consist typically of different anticipated/experienced transient load cases with altering temperature, pressure and flow rate. As the loading conditions concerning the LTCP are associated with temperatures considerably lower than that corresponding to the operational conditions, such load transients are to be considered that include this lower temperature region. Also the locally confined WRSs in the welds need to be taken into account. The dead weights of the analysed components can also be considered, however, in most cases their contribution to total stress distributions is only minor.

The two load transients encountered in PWR environments assumed here to include temperature region(s) associated with the LTCP phenomenon are:

- Shutdown, and
- Emergency cooling.

These two load transients, being those considered in the present analyses, are described in more detail in Section 4.2, whereas the assumed WRS distributions are described in Section 4.3.

As it is mainly the process fluid, in most cases water, that causes the experienced loads, it is also necessary to consider how they are transferred to NPP components. In case of pressure there is no delay, as the NPP components experience immediately how it alters. Heat transfer is another matter, as due to fluid mechanics phenomena there is a delay in how the temperature distributions in NPP component inner surfaces follow the altering of those concerning the moving process fluid. This transfer delay/efficiency is commonly expressed with the heat transfer coefficient. When its value is relatively high, i.e. of the scale of some thousands of

W/m^2K , the heat transfer delay is very short, and the outcome is comparable to having a temperature boundary condition. For the examined cases it was assumed that the heat transfer coefficient has a constant value of $5000 W/m^2K$, which is considered to be a reasonably conservative approximation. As for the temperature distributions across the component wall, they are obtained from the results of the heat conduction analysis, with using as part of the needed input data the temperature distributions in the NPP component inner surface.

4.2 Transient load cases

The two load transients encountered in PWR environments assumed here to include temperature region(s) associated with the LTCP phenomenon are described in the following.

Load transient Shutdown

The load transient Shutdown is such that both temperature and pressure are relatively slowly lowered from the operational values to approximately those corresponding to one atmosphere in room temperature. According to ref. [5] the typical rate of temperature change in PWRs during Shutdown varies between 10 to 20 °C/h, and thus the load transient duration is more than 10 hours. For this relatively slow load transient temperature is the leading load parameter, so as to achieve evenly lowering temperature distribution within the NPP component walls, whereas typically the rate of pressure change is faster. Here the temperature associated with the LTCP phenomenon is 55 °C [1]. When during Shutdown the temperature has lowered to this level, it is assumed that corresponding pressure is 25 bar and that the hydrogen content is high enough to cause LTCP. Also, it can be assumed that the Shutdown occurs yearly a few times.

Load transient Emergency cooling

Some types of malfunctions or accidents can cause the reactor pressure vessel (RPV) to suddenly fill with cool water or cause the reactor coolant water temperature to decrease rapidly. Mainly this occurs in case of loss-of-coolant-accident (LOCA). Such rapid Emergency cooling causes the RPV and connecting main nozzles to experience a thermal shock. If the RPV is then subjected to high pressure, the phenomenon is referred to as pressurised thermal shock (PTS). The Emergency cooling is assumed to occur much more seldom than the Shutdown, as plant specifically the number of experienced LOCAs during operational lifetime ranges typically from only a few to less than ten. For instance, the number of operational commercial NPP units worldwide at the beginning of 2010, being 437 according to ref. [8], divided by the number recorded leaks by the end of 2008, being 2158 according to ref. [9], is approximately 5.

In LOCA accident scenario it is postulated that a leak/break takes place in some NPP piping system component. The larger the break, the faster the load transient proceeds, and the more severe the cooling. Larger breaks cause a greater pressure decrease, which results in larger emergency core cooling (ECC) flows. This causes the RPV downcomer temperature to drop rapidly. The rate of temperature decrease and the minimum temperature achieved are the dominant thermal-hydraulic factors that influence the severity of the transient [6].

As compared to Shutdown the duration of the Emergency cooling is much shorter, thus it may cause significant temperature gradients across component walls. In the following are presented for two PWR NPPs in the U.S. the simulated Emergency cooling load transients corresponding to LOCAs of different sizes, see Figures 4.2-1 to 4.2-4. The thermal-hydraulic simulations were carried out with 5th version of the RELAP5 code [7], and the examined location is the upper part of the RPV downcomer.

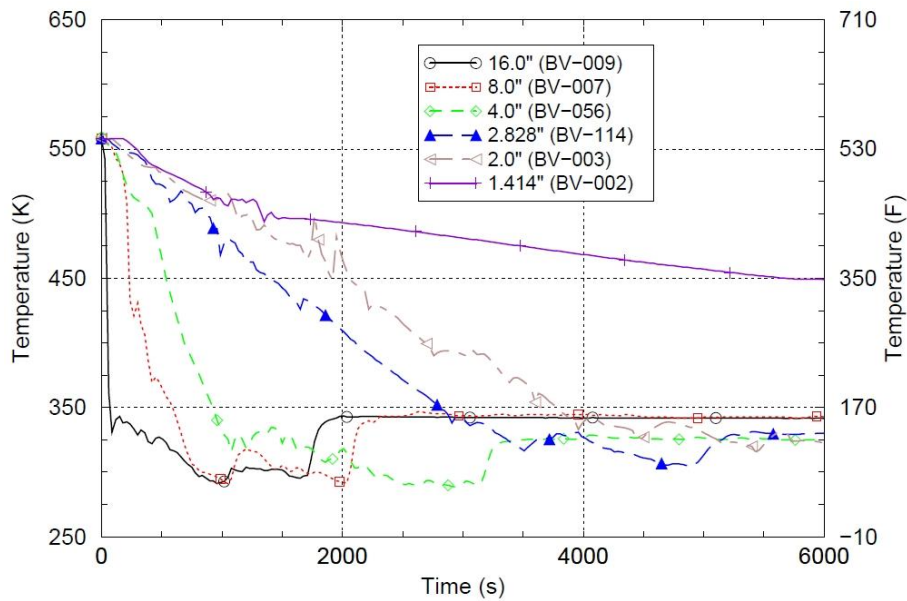


Figure 4.2-1. Simulated effect of surge line and hot-leg break diameter in case of Emergency cooling for RPV downcomer temperature in Beaver Valley PWR NPP unit [6].

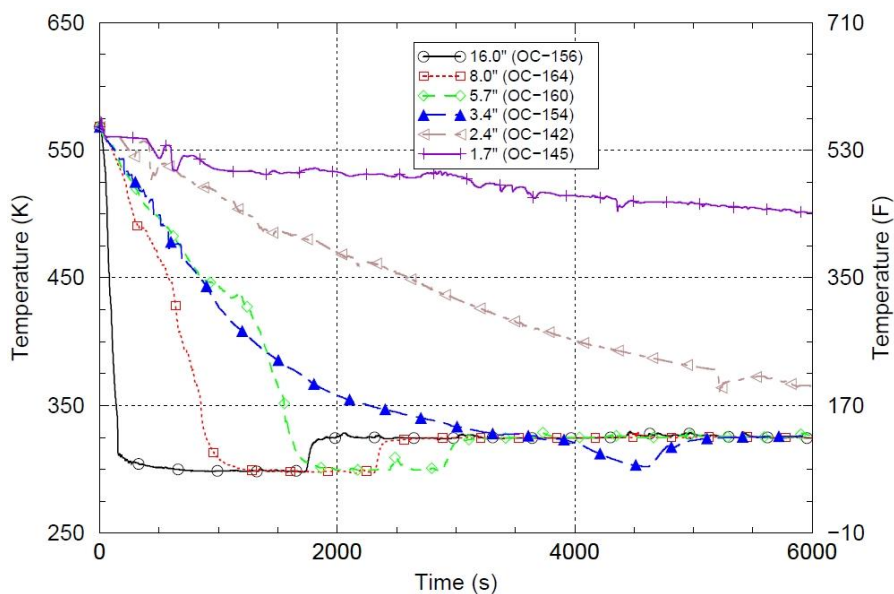


Figure 4.2-2. Simulated effect of surge line and hot-leg break diameter in case of Emergency cooling for RPV downcomer temperature in Oconee PWR NPP unit [6].

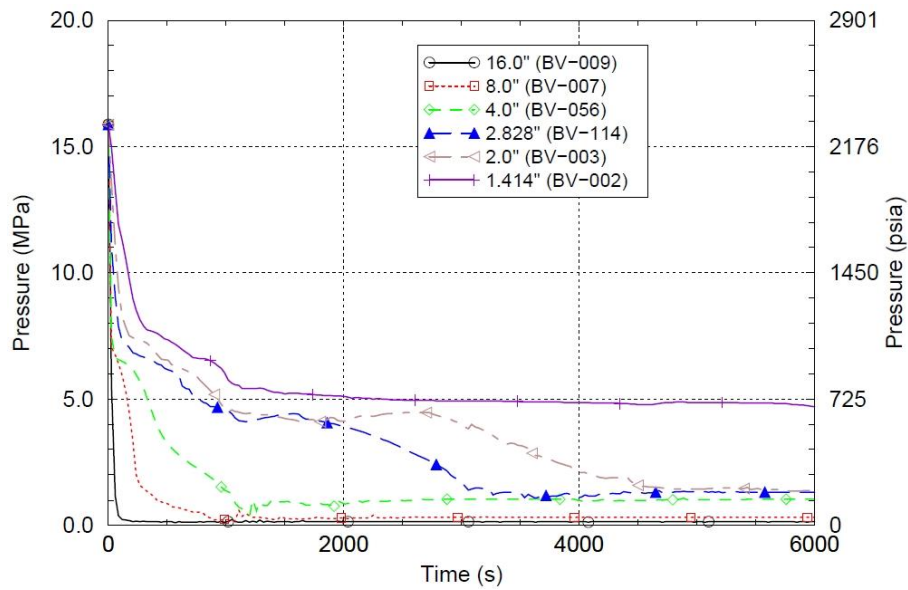


Figure 4.2-3. Simulated effect of surge line and hot-leg break diameter in case of Emergency cooling for RPV downcomer pressure in Beaver Valley PWR NPP unit [6].

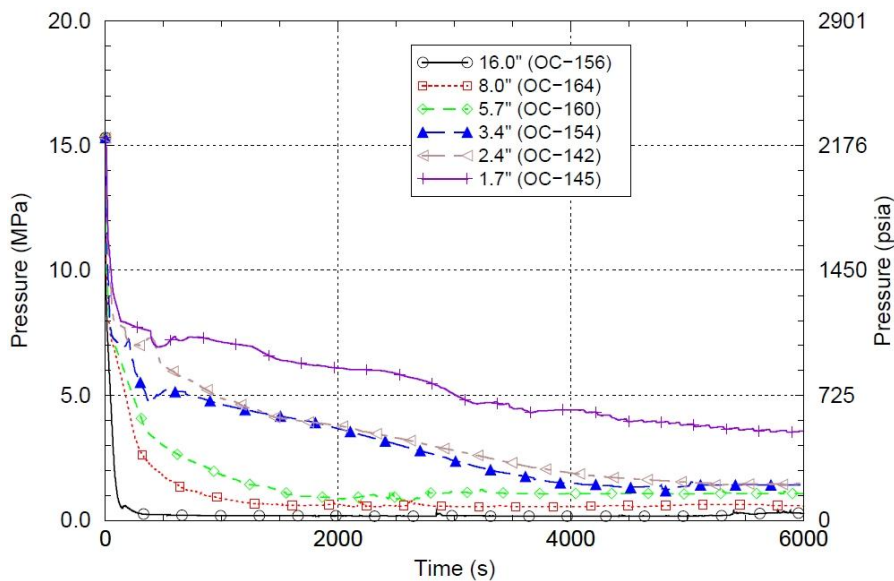


Figure 4.2-4. Simulated effect of surge line and hot-leg break diameter in case of Emergency cooling for RPV downcomer pressure in Oconee PWR NPP unit [6].

Concerning both of the above presented Emergency cooling load transients, the variations in injection water temperature occur both at the time when the volume of the refueling water storage tank is exhausted and when the high/low-pressure safety injection pumps start drawing off the containment sump (being a water reservoir located below the RPV). The sudden increase in the downcomer temperature evident at approximately 2000 s on the 8 and 16 inch diameter break curves in the Figures 4.2-3 and 4.2-4 indicate the time at which the switch-over to the containment sump occurs.

The second largest break presented in the Figures 4.2-1 to 4.2-4 is selected for further steps of computation, as it provides a clear and distinctive enough contrast in comparison to relatively slow Shutdown. The tabulated approximate temperature and pressure values for this 8.0", i.e. 203 mm, diameter pipe break Emergency cooling load transient are presented in Table 4.2-1 in the following for both NPP units in question. As in case of the Beaver Valley NPP unit this load transient is more severe than for the Oconee NPP unit, the former is selected to be used in further computations. When during Emergency cooling the temperature has lowered to this level, it is assumed that the hydrogen content is high enough to cause LTCP.

Table 4.2-1. The approximate simulated RPV temperature and pressure values for 8.0", i.e. 203 mm, diameter pipe break emergency cooling load transient for Beaver Valley and Oconee NPP units [6].

Time [s]	Beaver Valley			Oconee	
	Temperature [°K]	Temperature [°C]	Pressure [MPa]	Temperature [°K]	Pressure [MPa]
0	560	287	15.5	560	15.5
100	550	277	6.5	540	6.5
200	535	262	5.0	520	5.0
300	420	147	1.3	490	3.2
400	400	127	1.1	480	2.3
500	370	97	0.9	460	1.9
600	350	77	0.6	450	1.6
700	325	52	0.4	410	1.3
1000	285	12	0.3	310	1.1
1100	315	42	0.2	305	0.6
1300	310	37	0.1	300	0.4
1500	305	32	0.1	300	0.3
1700	295	22	0.1	300	0.3
1800	290	17	0.1	300	0.3
1900	290	17	0.1	300	0.3
2000	280	7	0.1	300	0.3
2100	300	27	0.1	300	0.3
2300	330	57	0.1	300	0.3
2400	340	67	0.1	325	0.3
6000	340	67	0.1	325	0.3

4.3 Welding process induced residual stresses

The welding process induced residual stresses in the welds that have not been in the PWHT are usually quite high, often of the scale of yield stress in and near the component surfaces, see e.g. ASME recommendations [16] for axial and circumferential residual stress distributions for pipe component welds. The PWHT, on the other hand, would lower the WRSs to a considerable extent. Here it is assumed that the examined DMW has not been in PWHT.

Applicable WRS distributions for the analysed DMW were obtained from the SSM handbook [17], see Appendix R. The SSM handbook [17] has been prepared for safety assessments of components with cracks and for assessments during the interval between the inspections of

components in NPPs. From the cases presented in the Appendix R of ref. [17] it is the WRSs for the Butt-welded bimetallic pipes (V or U shape) that is used here.

The magnitudes of the WRSs are expressed in relation to stress quantity S_r [N/mm^2], which is set to 0.2 % strain material yield stress at the considered temperature. For austenitic alloys, however, S_r , should be chosen as 1.0 % proof stress at the considered temperature. This is mainly due to the substantial strain hardening that occurs for austenitic alloys. When data concerning 1.0 % proof stress are not available, it may be estimated to be 1.3 times the corresponding 0.2 % proof stress [17].

Applicable dissimilar weld types for which WRS distributions in the pipe weld centre-line and HAZs are defined

The recommendations of the WRS distributions given here are based on a numerical investigation and apply to girth welds applied from the outside (single sided V or U preparation), see Figure 4.3-1. The material at HAZ appears to have little influence on residual stresses. The position (left or right) decides the magnitude and the distribution of the residual stress.

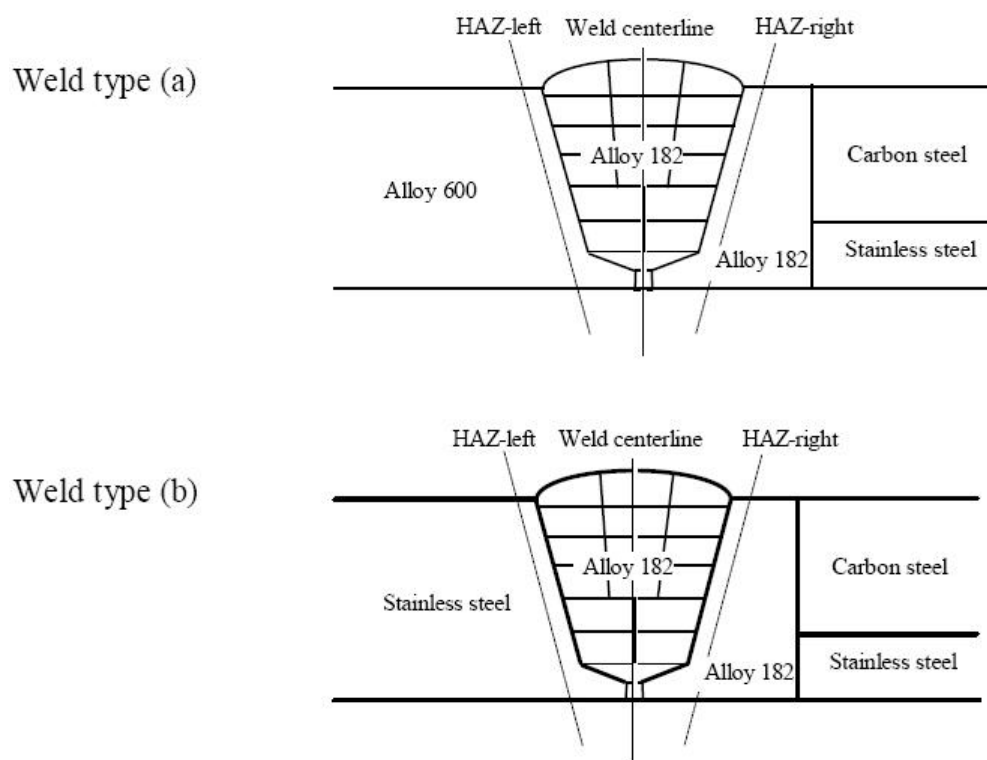


Figure 4.3-1. Applicable dissimilar weld types (a) and (b) in the SSM handbook [17] for which WRS distributions in the pipe weld centre-line and HAZs are given.

Axial and circumferential WRS distributions in the pipe weld centre-line and HAZs for dissimilar welds

The WRSs across the thickness, σ [N/mm²], are fitted by a fifth degree polynomial as follows [17]:

$$\sigma = c_0 + \sum_{i=1}^5 c_i \cdot \left(\frac{u}{t}\right)^i \quad (4.3-1)$$

where u [mm] is radial coordinate through wall with origin at the inner surface and t [mm] is pipe wall thickness. The parameters for the recommended WRSs are presented in Tables 4.3-1 and 4.3-2 at three different cross lines, namely at the weld centre-line, the HAZ-left line and the HAZ-right line, respectively.

Table 4.3-1. Coefficient values, c_i , for using equation (4.3-1) to define recommended axial (transverse) WRSs for butt welded bi-metallic dissimilar pipe weld joints, according to the SSM handbook [17].

Position	t [mm]	c_0	c_1	c_2	c_3	c_4	c_5
HAZ left	$t < 10$	245.0	539.8	-5734.5	12197.0	-11190.0	3849.1
weld centre		171.2	1257.6	-7048.2	11265.0	-8498.5	2570.4
HAZ right		253.4	188.3	-4357.1	7951.5	-5555.0	1396.4
HAZ left	$10 < t \leq 20$	129.3	26.2	-2066.3	7944.4	-11395.0	5175.9
weld centre		124.1	934.6	-9166.4	24979.0	-28074.0	11005.0
HAZ right		149.9	-800.3	1694.4	-2322.8	1724.8	-477.1
HAZ left	$20 < t \leq 30$	52.4	66.6	-5063.3	21002.0	-28115.0	11925.0
weld centre		100.7	-50.1	-5156.3	18102.0	-20949.0	7833.0
HAZ right		140.2	-1192.8	1868.0	1848.7	-6318.7	3782.3
HAZ left	$30 < t \leq 70$	33.0	-466.4	-4326.5	21424.0	-27647.0	10915.0
weld centre		32.9	-177.4	-5280.1	20579.0	-24143.0	8986.1
HAZ right		102.3	-1682.4	4191.1	-610.9	-6619.8	4881.2

Table 4.3-2. Coefficient values, c_i , for using equation (4.3-1) to define recommended circumferential (longitudinal) WRSs for butt welded bi-metallic dissimilar pipe weld joints, according to the SSM handbook [17].

Position	t [mm]	c_0	c_1	c_2	c_3	c_4	c_5
HAZ left	$t < 10$	187.9	38.7	107.8	-1831.0	1993.9	-512.8
weld centre		371.6	451.6	-1071.9	-1044.7	2504.2	-1151.1
HAZ right		197.8	523.3	-806.1	-2881.9	5462.9	-2457.7
HAZ left	$10 < t \leq 20$	248.2	297.3	-1696.1	5125.5	-7120.0	3173.0
weld centre		386.1	671.7	-6490.3	17792.0	-19862.0	7662.3
HAZ right		170.4	-315.5	1117.5	-1624.8	745.4	-14.3
HAZ left	$20 < t \leq 30$	252.2	-231.7	-354.8	5424.9	-9185.7	4174.3
weld centre		172.5	-658.2	2458.6	-159.7	-3635.1	2046.1
HAZ right		89.9	-596.9	4191.8	-6975.5	3644.5	242.7
HAZ left	$30 < t \leq 70$	16.4	-605.3	812.7	9426.8	-18206.0	8689.4
weld centre		88.7	170.4	-2984.4	13346.0	-17190.0	6833.8
HAZ right		91.9	273.8	-2184.1	11029.0	-16671.0	7719.9

5 Heat transfer and stress analyses

5.1 Overview of performed heat transfer and stress analyses

An overview of performed heat transfer and stress analyses is presented in the following. Of the two considered load transients, Shutdown and Emergency cooling, only in case of the latter one it was necessary to perform a heat transfer analysis. In case of Shutdown the changing of temperature was so slow, i.e. at maximum 20 °C/hour, that throughout its duration the temperature gradient across the wall was in practice negligible.

As both the assumed geometry, i.e. a DMW at a nozzle/safe-end joint, and applied loading are cylinder symmetric, it was possible to use analytical equations in the computations and a more straightforward analysis code. Also, only one material, being Alloy 182, was considered in the analyses.

In case of the load transient Shutdown it is sufficient to use analytical stress equations for straight pipe geometry under inner pressure load, as given in ref. [11]. Whereas in case of the load transient Emergency cooling the temperature and stress distributions across the wall as a function of time were computed with analysis code DIFF [10], which has been developed at VTT.

It was selected to terminate the transient analyses with DIFF when steady state conditions were reached. Steady state was defined by the temperature change rate: when the temperature at every temperature degree of freedom changes at a rate that is less than the specified rate, the analysis terminates. A suitably small value for the temperature change rate was chosen for the analyses, in all cases 1 °C or less. In the analyses the stress free temperature was assumed as 325 °C.

Main results from the heat transfer and stress analyses are presented in Section 5.4.

5.2 Applied analytical stress computation equations

For straight cylinder shaped components under inner pressure loading only, it is also possible to use straight forward analytical equations for computation of axial and circumferential stress distributions over the component wall. These equations are presented in the following.

The equation for axial stress distribution caused by inner pressure, $\sigma_{\text{AXIAL},p}$ [N/mm²], is for a straight pipe as follows [11]:

$$\sigma_{\text{AXIAL},p} = \frac{p \cdot R_i^2}{R_o^2 - R_i^2} \quad (5.2-1)$$

The equation for circumferential stress distribution caused by inner pressure, $\sigma_{\text{CIRC},p}$ [N/mm²], is for a straight pipe as follows [11]:

$$\sigma_{\text{CIRC},p} = \frac{p \cdot R_i^2}{R_o^2 - R_i^2} \cdot \left(1 + \frac{R_o^2}{r^2} \right) \quad (5.2-2)$$

where p [N/mm²] is inner pressure, R_i [mm] is inner radius, R_o [mm] is outer radius and r [mm] is radial coordinate through wall.

5.3 Analysis code DIFF

The description of the heat transfer and stress analysis code DIFF presented here is based on ref. [10]. The analysis code has been primarily developed to analyse the effects of pressurised thermal shocks in RPVs. However, the code can also be applied to any straight hollow cylinder, e.g. to pipes.

The temperature distributions in the structure induced by thermal transients are solved as a function of time with finite difference method in axially symmetric geometry. All material properties can be time dependent. The values of flow temperatures and heat transfer coefficients can be freely defined as a function of time. The base material and cladding layers of the component wall are defined as separate materials. The possible differing temperature zones of the coolant are defined in a simplified way so that the temperature distributions of the zones are solved as two separate and adjacent axially symmetric fields. The stress distributions are solved based on linear material behaviour, separately for the cladding cylinder and the base material cylinder with analytical equations for a cylinder having a thick wall. Then the solutions are matched together by demanding the fulfilment of the continuity terms at the interface surface. The effect of inner pressure is also added to the resulting stress distributions. The stress free temperature of the bimetal structure in question is also given as a part of the input data, so the effect of this property to the resulting stress distributions is taken into account as well.

The output data from DIFF analyses for the examined structure are the temperature distribution in radial direction and stress distributions in both axial and circumferential directions, all of which in numerical and graphical formats. The code makes an assessment of the time step given by the code user, and also checks the stability of the solution during the analysis. In addition, the code checks also other input data values and if necessary presents warnings, or in impossible calculation cases error notices, in which case it also stops the analysis process.

The verification of DIFF has been carried out by comparing the results from test analysis cases to the available analytical solutions or to solutions computed with common general purpose finite element method (FEM) codes.

5.4 Summary of heat transfer and stress analysis results

A summary of the obtained heat transfer and stress analysis results is presented in the following. As mentioned earlier, the analyses were performed using both analytical stress computation equations and analysis code DIFF. The results concerning load transient Shutdown are presented

first, then those corresponding to load transient Emergency cooling, then the WRS distributions as obtained according to the SSM handbook [17] assumptions, and finally the total stress distributions which combine all of the afore mentioned stress components. The results are shown as a function of time and/or distance through wall at DMW centre-line and right/left side HAZ, as case specifically suitable.

Stresses caused by load transient Shutdown

As during the Shutdown the rate of temperature change in PWRs is only of the scale of 10 to 20 °C/h, no temperature gradient through wall of the assumed DMW resulted. Thus the stresses through wall were simply computed for the pressure corresponding to the temperature associated with the LTCP, which is 55 °C [1], as mentioned earlier. The axial and circumferential stresses through wall of the examined DMW at that time instant from the duration of the Shutdown which corresponds to the LTCP conditions in the assumed PWR environment are shown in Figure 5.4-1 in the following.

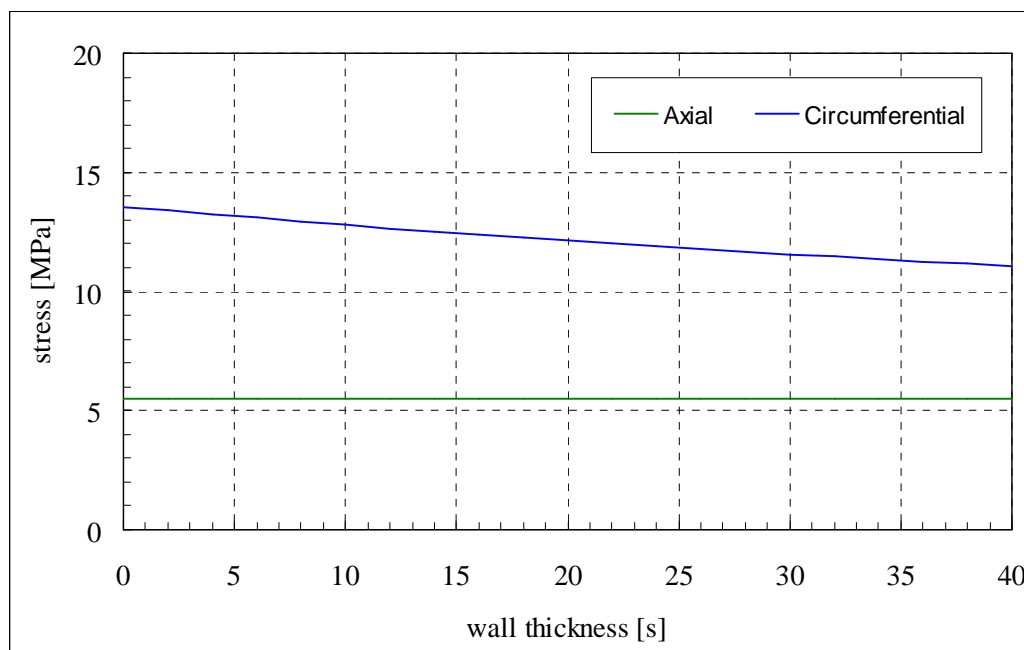


Figure 5.4-1. The axial and circumferential stresses through centre-line of the examined DMW at that time instant from the duration of the Shutdown which corresponds to the LTCP conditions in the assumed PWR environment. The horizontal axis presents a radial coordinate through wall with origin at the inner surface.

Stresses caused by load transient Emergency cooling

As during the Emergency cooling the rate of temperature change in the assumed PWR environment is remarkable, this necessitated to include in the analyses the computation of the temperature gradients through DMW wall. Thus both temperatures and stresses through wall were computed for the whole duration of the load transient to obtain the correct values

corresponding to the temperature associated with the most severe LTCP, which is 55 °C [1], as mentioned earlier. The temperature distributions through wall at the examined DMW are shown as a function of time for the duration of the Emergency cooling in Figure 5.4-2 in the following. As can be seen from this figure, the temperature at both the inner and outer surface reach the value of 55 °C twice during the load transient in question. The axial and circumferential stress distributions of the examined DMW are shown as a function of time for the duration of the load transient in question in Figures 5.4-3 and 5.4-4 in the following. Whereas the axial and circumferential stresses through wall of the examined DMW as corresponding to the LTCP conditions in the assumed PWR environment are shown in Figure 5.4-5. Of the mentioned two times that the DMW surface temperatures reach 55 °C, only the first time is considered here, as at the second time the resulting stresses are much lower. Also, it can be noted from the stress result figures that the axial and circumferential stresses have quite matching resulting values.

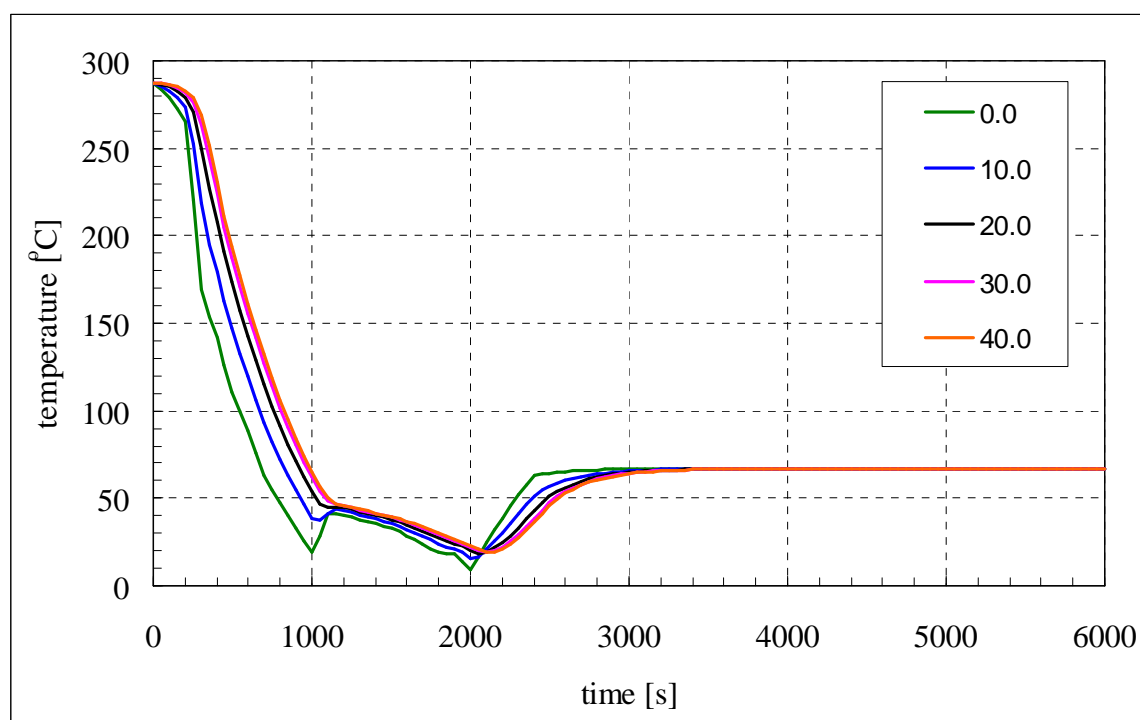


Figure 5.4-2. The temperature against time curves at selected points in centre-line of the examined DMW for the Emergency cooling. In the legend the values correspond to radial coordinate values through wall with unit of mm and origin at the inner surface.

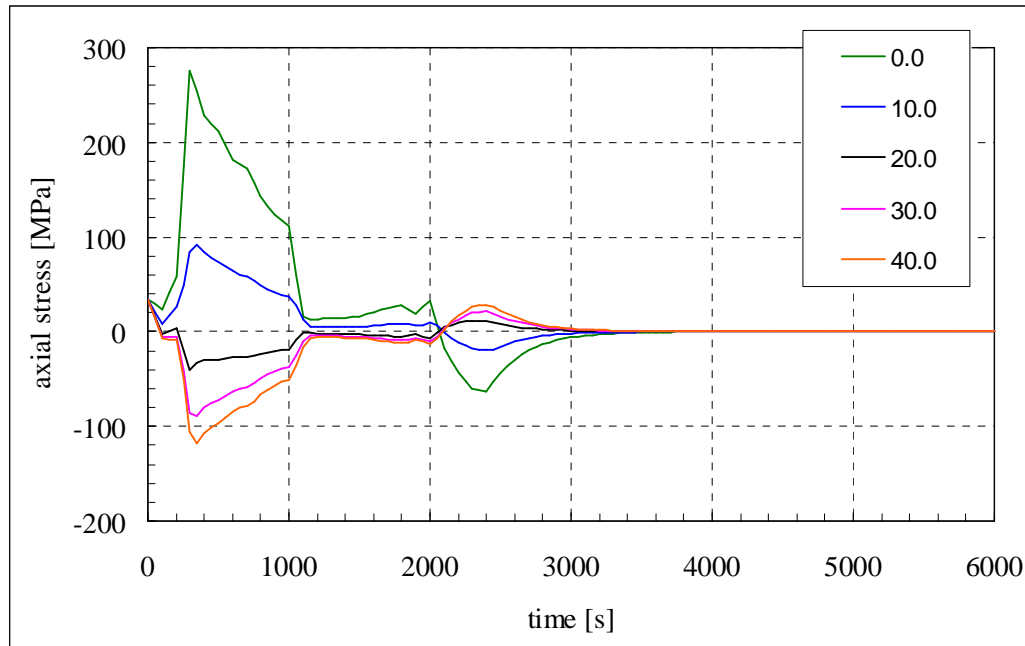


Figure 5.4-3. The axial stress against time curves at selected points in centre-line of the examined DMW for the Emergency cooling. In the legend the values correspond to radial coordinate values through wall with unit of mm and origin at the inner surface.

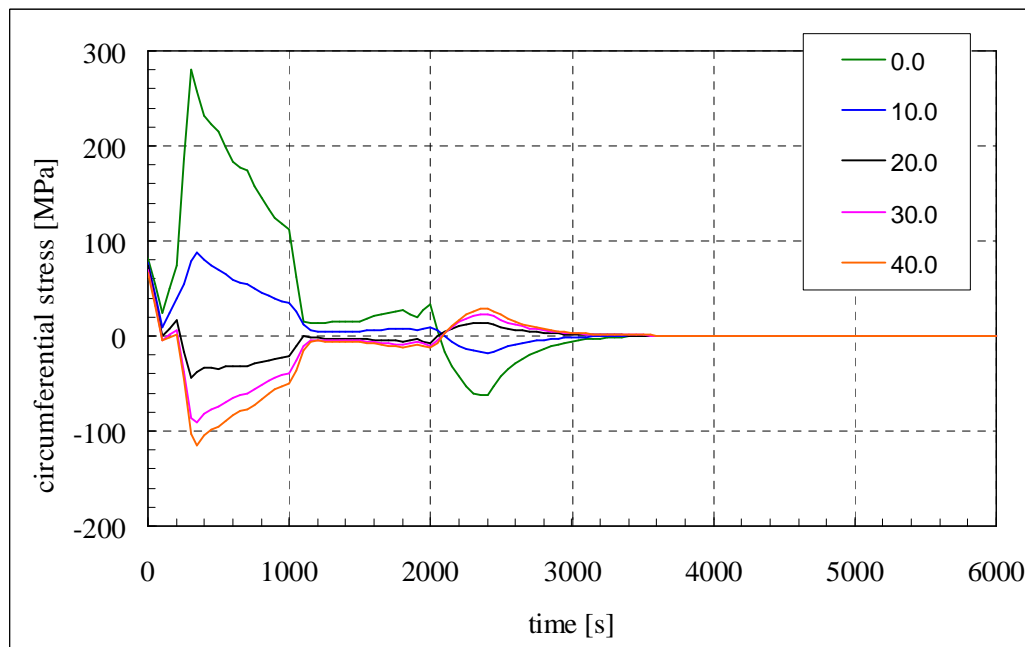


Figure 5.4-4. The circumferential stress against time curves at selected points in centre-line of the examined DMW for the Emergency cooling. In the legend the values correspond to radial coordinate values through wall with unit of mm and origin at the inner surface.

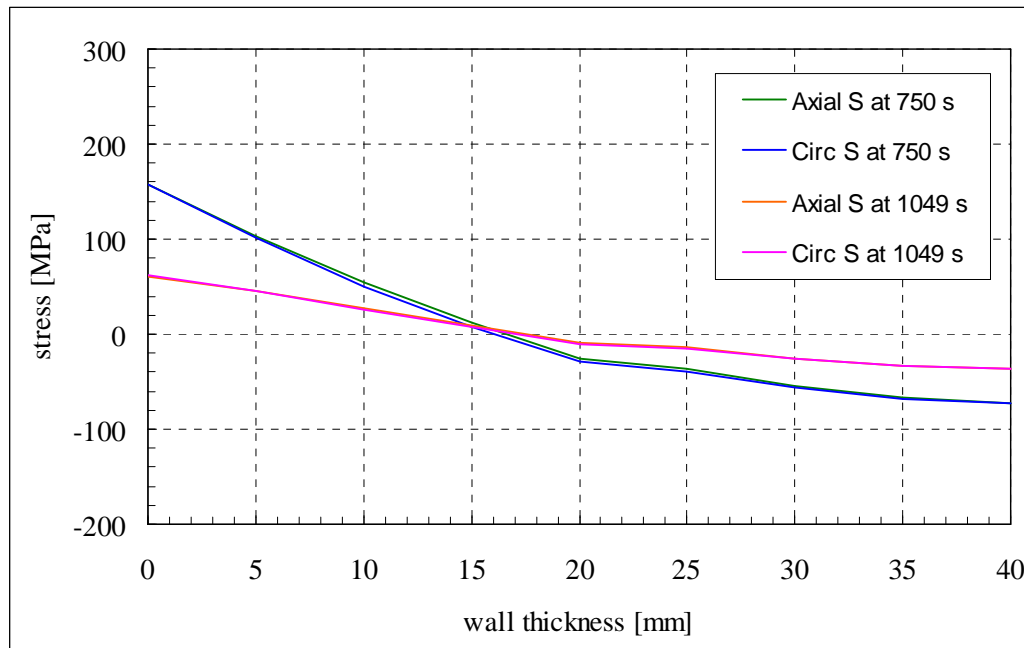


Figure 5.4-5. The axial and circumferential stresses through centre line of the examined DMW at the first of the two time instants from the duration of the Emergency cooling which corresponds to the LTCP conditions in the assumed PWR environment. The horizontal axis presents a radial coordinate through wall with origin at the inner surface. In the legend 750 s corresponds to the time the inner surface first reaches 55 °C, and 1049 s that when the outer surface reaches it, respectively.

Welding residual stresses according to SSM handbook assumptions

The WRSs as computed according to the SSM handbook [17] assumptions are presented in the following. More precisely, it is the axial and circumferential WRSs through wall of the examined DMW at weld centre line as well as at right and left side HAZs that are covered. These WRSs are both time and, for the considered variation region of load conditions, also temperature dependent. The WRSs are shown in Figures 5.4-6 and 5.4-7 in the following. In the legends of these figures HL is left side HAZ, CL is weld centre-line and HR is right side HAZ, respectively.

It is also noted here, that of the commonly applied fitness-for-service procedures only the SSM handbook [17] provides for the time being WRS assumptions also for DMWs, as e.g. R6 Method Rev. 4, SINTAP procedure, BS-7910 and FITNET procedure cover for pipe geometries WRSs only for similar welds.

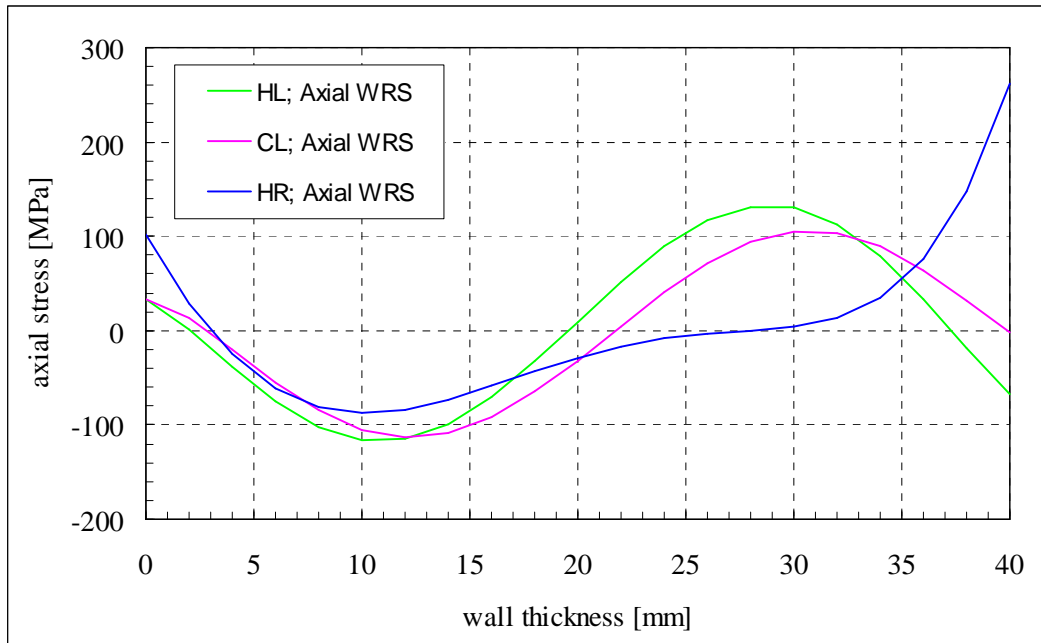


Figure 5.4-6. The axial WRSs through wall of the examined DMW as computed according to the SSM handbook assumptions [17]. The horizontal axis presents a radial coordinate through wall with origin at the inner surface.

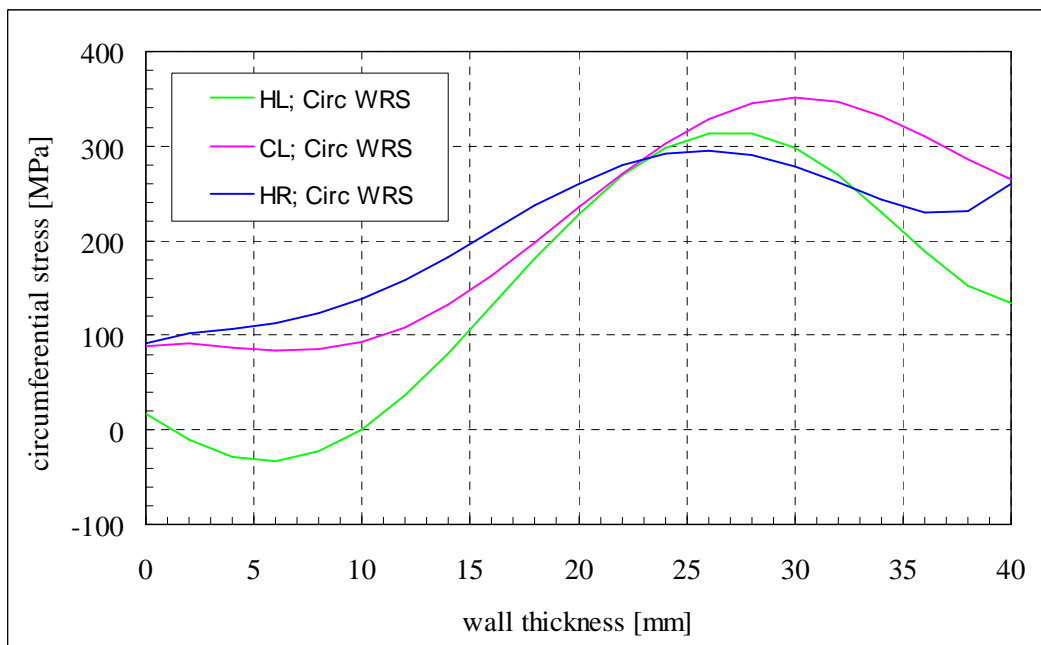


Figure 5.4-7. The circumferential WRSs through wall of the examined DMW as computed according to the SSM handbook assumptions [17]. The horizontal axis presents a radial coordinate through wall with origin at the inner surface.

Total stress distributions

The total stress distributions which combine all stress components as caused by the Shutdown, Emergency cooling and the WRSs are presented in the following. As concerning the two considered load transients, the total stress results are presented at that time instant from the duration of both of them that corresponds to the LTCP conditions in the assumed PWR environment, i.e. temperature of 55 °C. In case of the Emergency cooling there are two such time instants, for only the first of which the stress results are presented, as at the second of these time instants the stress components are in comparison much lower. The axial and circumferential total stresses through wall of the examined DMW at weld centre-line as well as at right and left side HAZs that are shown in Figures 5.4-8 to 5.4-10 in the following. In the legends of these figures HL is left side HAZ, CL is weld centre-line and HR is right side HAZ, respectively.

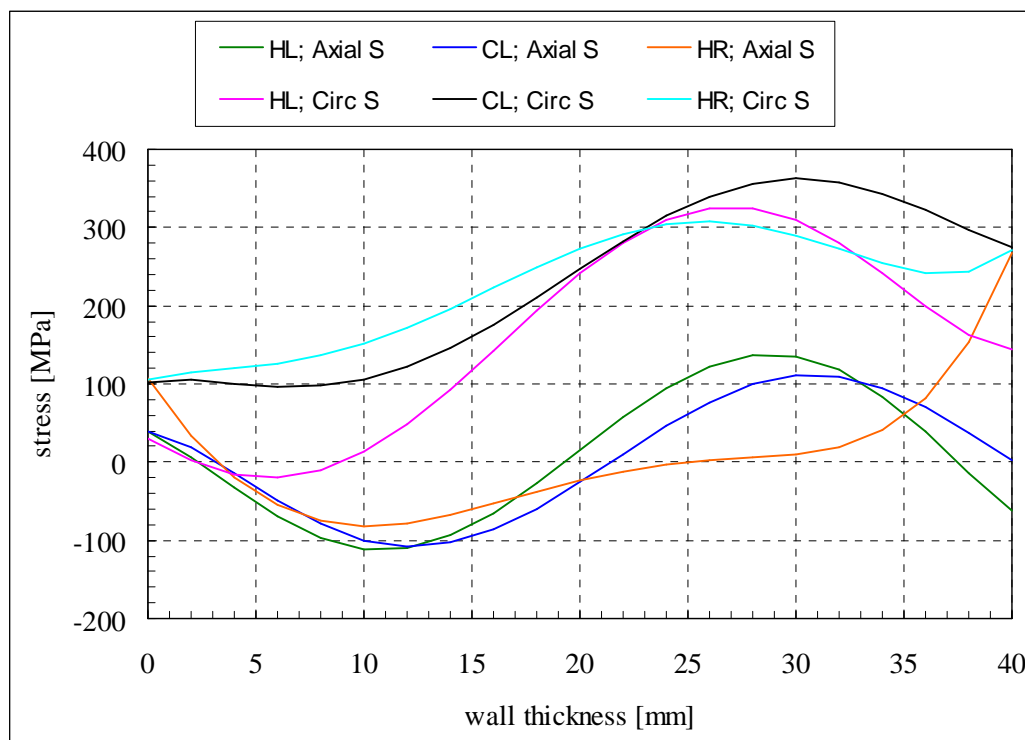


Figure 5.4-8. The axial and circumferential total stresses through DMW wall at the time instant from the duration of the Shutdown which corresponds to the LTCP conditions. As horizontal axis is radial coordinate through wall with origin at the inner surface.

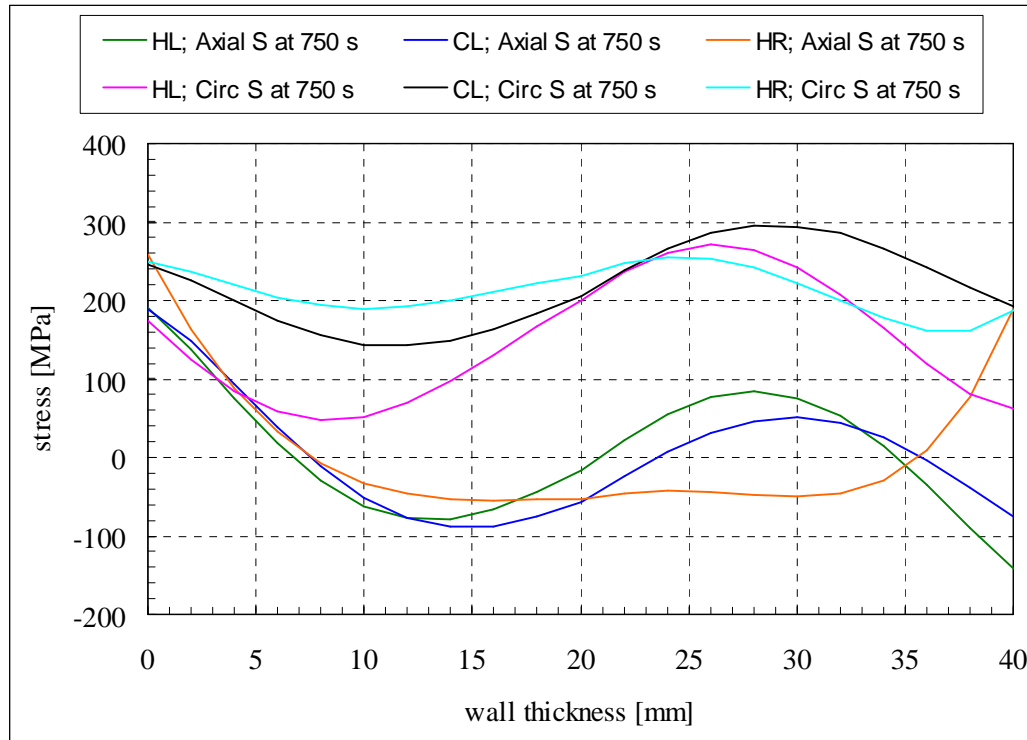


Figure 5.4-9. The axial and circumferential total stresses through DMW wall at the first of the two time instants from the duration of the Emergency cooling which corresponds to the LTCP conditions. As horizontal axis is radial coordinate through wall with origin at the inner surface. In the legend 750 s corresponds to the time the inner surface first reaches 55 °C.

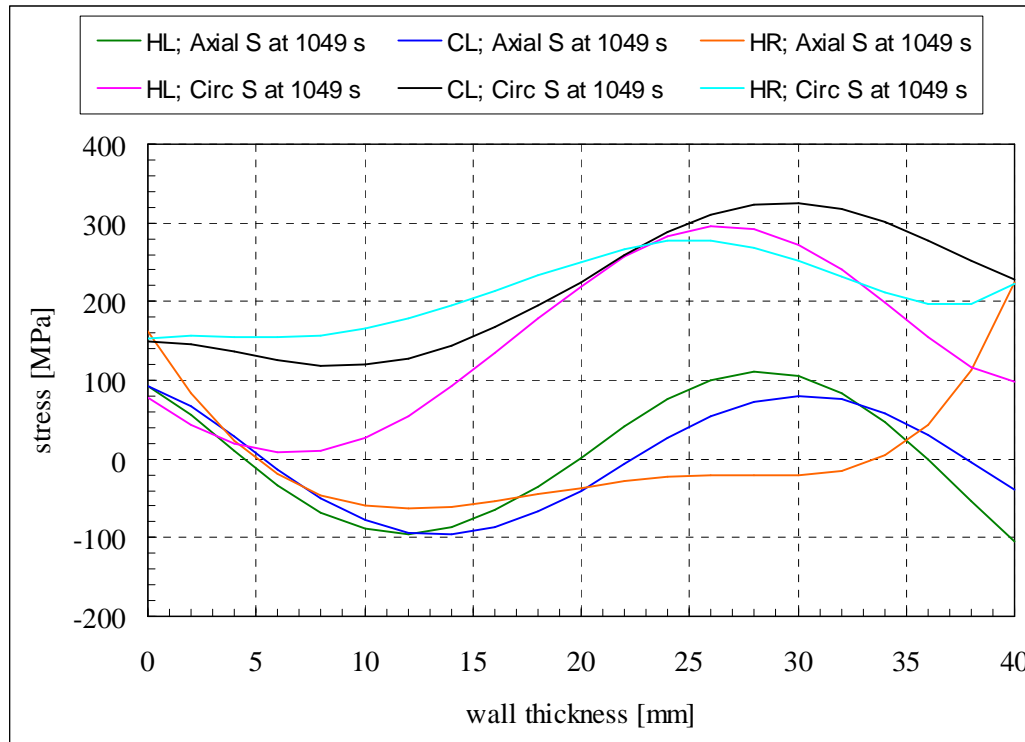


Figure 5.4-9. The axial and circumferential total stresses through DMW wall at the first of the two time instants from the duration of the Emergency cooling which corresponds to the LTCP conditions. As horizontal axis is radial coordinate through wall with origin at the inner surface. In the legend 1049 s corresponds to the time the outer surface reaches 55 °C.

6 Crack sensitivity analyses and their results

6.1 Analysed crack postulates and associated input data

In this study the structural integrity analyses were performed to a DMW at a nozzle/safe-end joint resembling that in PWR plants. As mentioned earlier in Chapter 2, the considered crack postulate type is an inner axially oriented semi-elliptic surface crack in the weld material. For overall shape of the crack postulate type, used geometry parameters and characteristic points, see Figure 6.1-1 in the following.

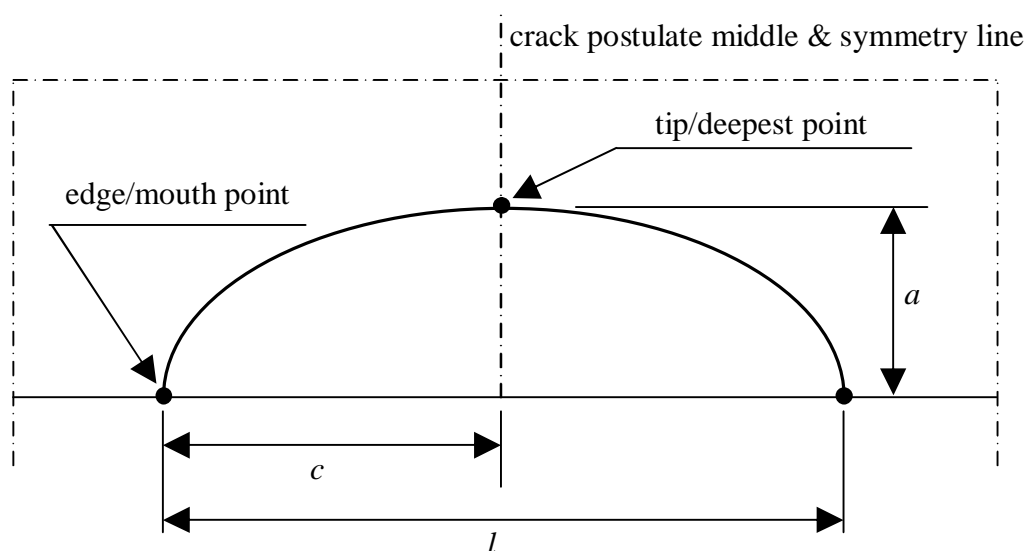


Figure 6.1-1. For a semi-elliptic surface crack, the overall shape, used geometry parameters and characteristic points. Here a [mm] is crack postulate depth, l [mm] its length, and c [mm] half of the latter, whereas a/c is called the aspect ratio, respectively.

The following Table 6.1-1 presents the crack sensitivity analysis cases for the assumed DMW at a nozzle/safe-end joint. Also presented are loads, and as there are three loading cases for each of the four crack postulates, altogether 12 analysis cases results. Here no particular crack growth mechanism is assumed. Concerning the two considered load transients, those time instants from their duration which correspond to the LTCP conditions are taken into account in the analyses. For all crack sensitivity analysis cases the WRSs according to the SSM handbook [17] assumptions are included as such. Thus in the crack sensitivity analyses it is the total stresses consisting both of load transient and WRS components that are applied. Also, as component dimensioning was not an issue here, no safety factors were applied.

Besides the crack postulate and load data in the Table 6.1-1, the rest of the input data needed in the crack sensitivity analyses are presented in detail in Chapters 2, 3 and 5, respectively.

Table 6.1-1. The considered 12 crack sensitivity analysis cases for the assumed DMW. Three loading cases for each of the four crack postulates.

Case No.	Location	Surface	Orientation	Aspect ratio	Load cases
1 - 3	Weld, middle	Inner	Axial	1/1	Shutdown, Emergency cooling at 750 and 1049 s
4 - 6	Weld, middle	Inner	Axial	1/3	Shutdown, Emergency cooling at 750 and 1049 s
7 - 9	Weld, middle	Inner	Axial	1/5	Shutdown, Emergency cooling at 750 and 1049 s
10 - 12	Weld, middle	Inner	Axial	1/10	Shutdown, Emergency cooling at 750 and 1049 s

6.2 Limiting crack sizes

As mentioned earlier, here no crack growth mechanism is assumed, as the main point is to find those crack sizes for which the crack tip value of a relevant fracture mechanics based cracking parameter equals the corresponding fracture toughness.

For the material considered here, Alloy 182, with a relatively large strain hardening region the fracture mode is ductile within the temperature range encountered in PWR plants. Of the fracture mechanics based cracking parameters, which are computed over the crack front, the often used stress intensity factor that mainly characterises linear-elastic material behaviour is not sufficient for describing ductile fracture, thus the J -integral developed specifically for this purpose is to be used. Typically as well as here it is the opening mode, i.e. mode I, fracture that is considered.

Thus the limiting criterion for crack size becomes here the computed maximum value of mode I J -integral reaching the corresponding mode I fracture toughness, being here J_{IC} , the values for which are obtained for the examined LTCP conditions from the main background document [1]. To get a wider scope of the distribution of the limiting crack size, it is computed for each of the aspect ratios and load cases mentioned in the Table 6.1-1.

6.3 Steps of performed crack sensitivity analyses

The steps of the performed crack sensitivity analyses are summarised here in the order of the computations. These elastic-plastic fracture mechanics based analyses were performed to the set of crack postulates presented in the Table 6.1-1 in Section 6.1. For each considered crack postulate aspect ratio such crack sizes were computed for which the crack tip values of elastic-plastic J -integral reaches the corresponding fracture toughness values, as given in the Table 3-4 in Section 3.4. Also, as mentioned earlier, no safety factors were applied in this study.

Step 1. Firstly in the crack sensitivity analyses, for each considered crack postulate aspect ratio the distributions of linear-elastic mode I stress intensity factor, K_I [MPa \sqrt{m}], values over the crack front were computed for a set of crack sizes ranging from relatively small, with $a = 1.0$ mm, to relatively large, with $a/t_w = 80-100$ %, respectively. These computations were performed with fracture mechanics based analysis code VTTBESIT, which is described in more detail in Section 6.4, and the needed input data are described in Section 6.1. In the VTTBESIT computations the stresses perpendicular to crack postulate surfaces were included for each case along three lines through wall, those being the weld centre-line as well as right and left side HAZs.

Step 2. Secondly, and based on the results obtained in the Step 1, are computed the plasticity corrected K_I values, denoted as K_{Ip} [MPa√m] values. To compute those and the effective crack depth, a_{eff} [mm], which is also needed in this connection, the following applicable equations from ref. [12] are used:

$$K_{Ip} = \sqrt{\frac{a_{eff}}{a}} \cdot K_I \quad (6.3-1)$$

and:

$$a_{eff} = a + \left(\frac{1}{2 \cdot \pi \cdot \beta} \right) \cdot \left(\frac{K_I}{S_y} \right)^2 \quad (6.3-2)$$

where β [-] is 1 for plane stress and 3 for plain strain, and the values for S_y are given in Chapter 2, respectively.

Step 3. The elastic values of J -integral, J_{el} [kJ/m²], are then computed as follows [14]:

$$J_{el} = \frac{K_{Ip}^2}{E'} \quad (6.3-3)$$

where $E' = E/(1-\nu^2)$ for plane strain, $E' = E$ for plane stress, and the values for E are given in Chapter 2, respectively.

Step 4. Next in turn is the computation of plastic values of J -integral, J_{pl} [kJ/m²], which is carried out as follows [14]:

$$J_{pl} = \mu \cdot K_I^2 \cdot \left(\frac{\varepsilon_{ref} \cdot P_L}{S_y \cdot P} - \frac{1}{E} \right) \quad (6.3-4)$$

where μ [-] is 1 for plane stress and 0.75 for plain strain, ε_{ref} [mm/mm] is reference strain computed according to the equation (6.3-5) in the following, P [MPa] is the inner pressure corresponding to prevailing loads and P_L [MPa] is the limit load as computed according R6 Method, Rev. 4 [12], Chapter IV, Subsection IV.1.9.2 “Axial internal rectangular/semi-elliptical defects in thick-walled cylinders” solution.

The reference strain is associated with reference stress, σ_{ref} [MPa], which computed according to equation in ref. [15] is also to be lower than S_y . Thus both the reference stress and reference strain belong to linear material behaviour region, and the latter can be now computed as follows:

$$\varepsilon_{ref} = \left(\frac{\sigma_{ref}}{S_y} \right) \cdot \varepsilon_y \quad (6.3-5)$$

where ε_y [mm/mm] = 0.2 % is yield strain corresponding to S_y .

Step 5. Finally, the elastic-plastic values of J -integral, J_{ep} [kN/m²], are computed as follows [14]:

$$J_{ep} = J_{el} + J_{pl} \quad (6.3-6)$$

6.4 Computer code used in fracture mechanics analyses

The fracture mechanics based K_I analyses were performed with the analysis code VTTBESIT. This analysis code comprises parts developed by the Fraunhofer-Institut für Werkstoffmechanik (IWM), Germany, and by VTT.

With VTTBESIT it is possible to calculate K_I values over the crack postulate fronts. The analysis code treats only the mode I loading (in which the direction of the loading is perpendicular to the crack surfaces, i.e. crack opening mode). These calculations are carried out with program BESIT60, developed by IWM. This program is based on the weight/influence function method. Solutions are provided for "infinite" and semi-elliptical surface crack postulate cases in straight plates and cylinders. The theoretical background and analysis procedures of BESIT60 are presented in refs. [18, 19, 20].

VTTBESIT uses the BESIT60 program code as a pure stress intensity factor value computing subroutine and applies the results as starting values for crack growth assessments as well as for the assessment of end-of-life crack sizes.

Material and geometry data needed for the computation are given through a graphical interface. The same data can also be given in a text file format. Loading data, in form of stress distribution through the component wall, are given in a separate file, the ending of which is *.spa. This file can be created with any common text editor. Loading data can be given as a function of time either in Cartesian or polar co-ordinates. Also, the stress data can be given along one or several lines through wall. In the former case the program assumes a one dimensional stress field, whereas in the latter case it is two dimensional with interpolation between the given values.

General information about the analysis (for example the name of the used analysis procedure) is given in a protocol file named example.ptl. The analysis code writes the results in a file TESTRES.OUT. To avoid losing the results, this file should either be copied with a different name or the results in the file should be copied for example into a spread sheet file. In case of a semi-elliptical surface crack postulate, the results are given at various locations along the crack front: $\phi = 0^\circ$ (first crack mouth), $\phi = 30^\circ$, $\phi = 60^\circ$, $\phi = 90^\circ$ (crack tip), $\phi = 120^\circ$, $\phi = 150^\circ$, and $\phi = 180^\circ$ (second crack mouth), where the origin of the angular crack front location parameter ϕ is in the midpoint of that symmetry axis of the semi-elliptic crack postulate which coincides with the component surface.

In the crack growth analyses with VTTBESIT it is also possible to calculate maximum allowable (i.e. end-of-life) crack sizes according to Section XI of the ASME code [21], as well as those crack sizes for which it would take 1, 2, 3, 4, 5, 6, 7, 8, 9 and 10 years to grow to these maximum allowable sizes. Two crack growth models are provided in the analysis code: Paris-Erdogan equation for fatigue induced crack growth, and rate equation for SCC. This crack growth analysis option was excluded from the scope of the present study.

In the present study only the K_I and crack size results from VTTBESIT computations are used in further steps of the crack sensitivity analyses.

6.5 Results from crack sensitivity analyses

The results from the crack sensitivity analyses are presented in the following. While the limiting criterion for crack size being here that the computed J_I value at the crack tip reaches the corresponding mode I fracture toughness, J_{IC} , it is mainly the J_I results against J_{IC} values that are presented here. All in all 12 crack analysis cases are covered, see the Table 6.1-1. Also, for J_{IC} there are three different values, see the Table 6.3-4.

As according to the analysis results the J_I values for the first three cases, having aspect ratio of 1/1, remained below 30 kJ/m^2 , i.e. below all considered J_{IC} values, these cases were omitted from the result presentation here. Also, the rise of the slope of the J_I results as a function of crack depth started to decrease and eventually the slope assumed a horizontal direction. It is however noted, that for this aspect ratio as well as for those with higher values, i.e. narrow cracks, the K_I values typically remain markedly low, and thus correspondingly also the consequent J_I values.

In the following are presented for the three cases with aspect ratio of 1/3 the J_I results against the J_{IC} values, see Figures 6.5-1 to 6.5-3. In the legends of these figures JIC-1 is J_{IC} value for $33 \text{ cm}^3 \text{ H}_2/\text{kg H}_2\text{O}$ without pre-exposure, JIC-2 is J_{IC} value for $100 \text{ cm}^3 \text{ H}_2/\text{kg H}_2\text{O}$ with pre-exposure, and JIC-3 is J_{IC} value for $100 \text{ cm}^3 \text{ H}_2/\text{kg H}_2\text{O}$ without pre-exposure, whereas 90° is crack tip location, respectively.

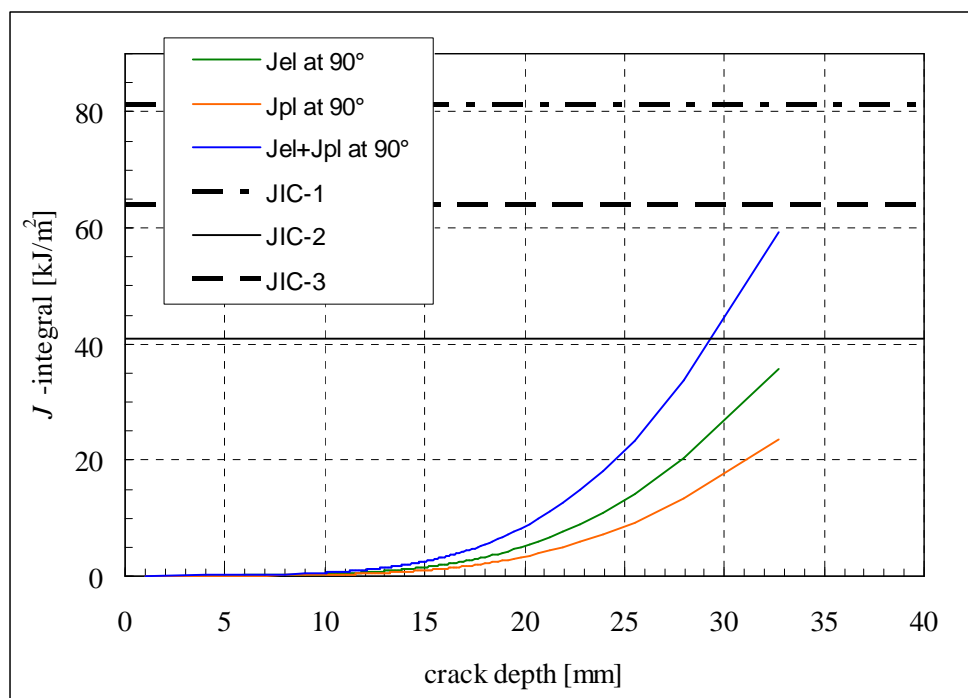


Figure 6.5-1. The J_I results against the J_{IC} values for inner axial semi-elliptical surface crack at assumed DMW; Case 4 with aspect ratio of 1/3.

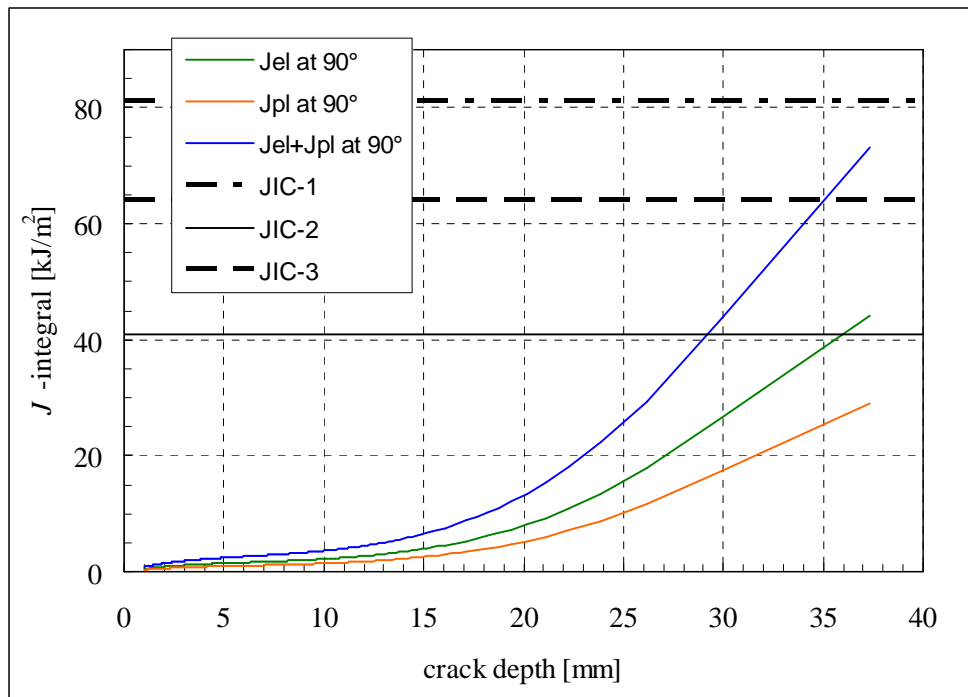


Figure 6.5-2. The J_I results against the J_{IC} values for inner axial semi-elliptical surface crack at assumed DMW; Case 5 with aspect ratio of 1/3.

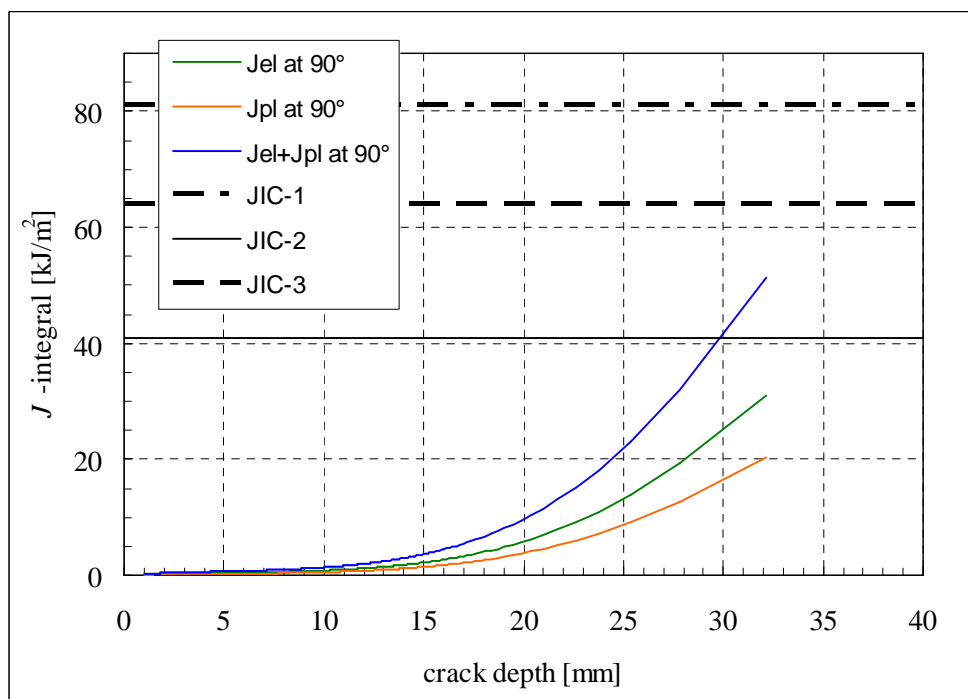


Figure 6.5-3. The J_I results against the J_{IC} values for inner axial semi-elliptical surface crack at assumed DMW; Case 6 with aspect ratio of 1/3.

In the following are presented for the three cases with aspect ratio of 1/5 the J_I results against the J_{IC} values, see Figures 6.5-4 to 6.5-6. In the legends of these figures JIC-1 is J_{IC} value for 33 cm³ H₂/kg H₂O without pre-exposure, JIC-2 is J_{IC} value for 100 cm³ H₂/kg H₂O with pre-exposure, and JIC-3 is J_{IC} value for 100 cm³ H₂/kg H₂O without pre-exposure, whereas 90 ° is crack tip location, respectively.

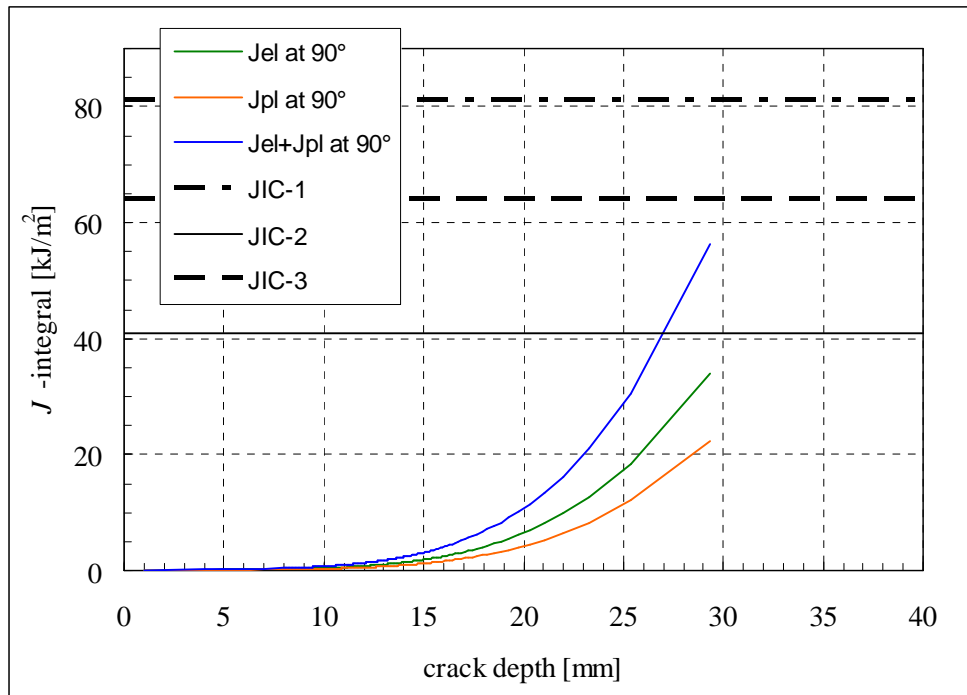


Figure 6.5-4. The J_I results against the J_{IC} values for inner axial semi-elliptical surface crack at assumed DMW; Case 7 with aspect ratio of 1/5.

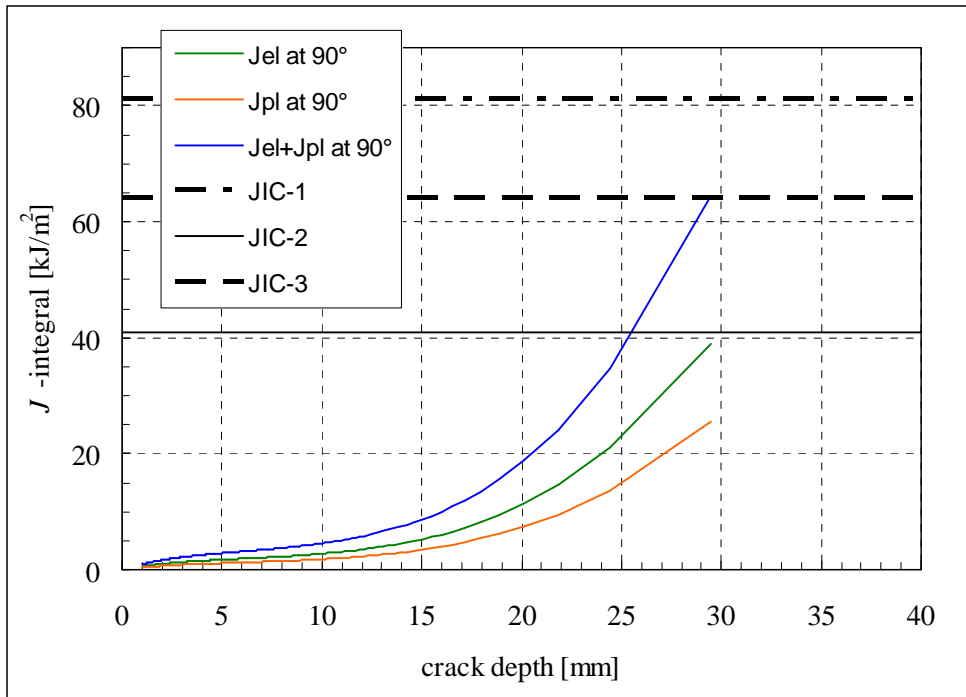


Figure 6.5-5. The J_I results against the J_{IC} values for inner axial semi-elliptical surface crack at assumed DMW; Case 8 with aspect ratio of 1/5.

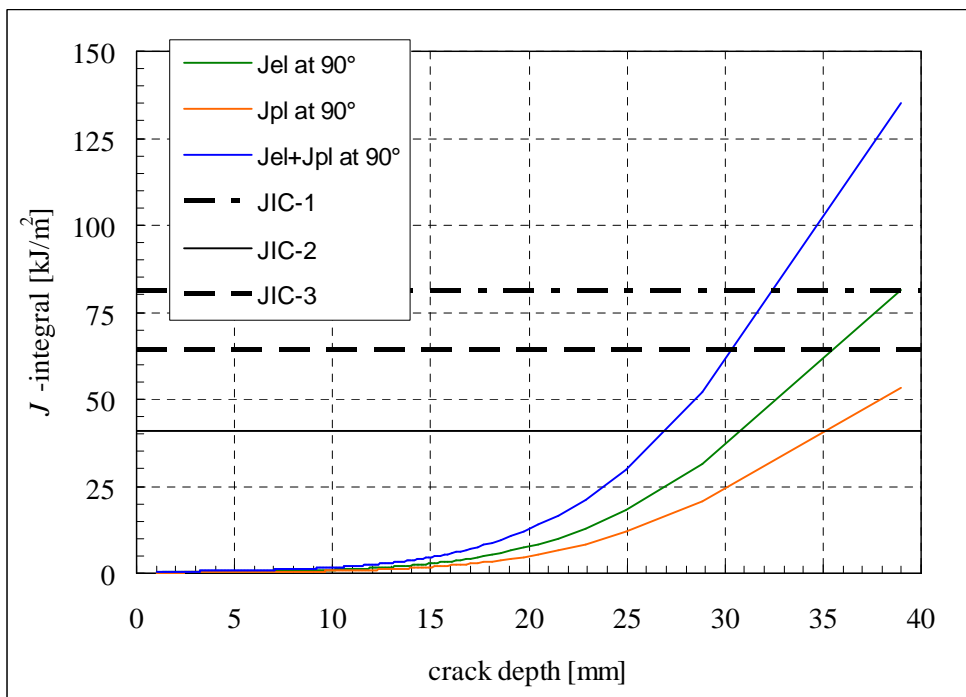


Figure 6.5-6. The J_I results against the J_{IC} values for inner axial semi-elliptical surface crack at assumed DMW; Case 9 with aspect ratio of 1/5.

In the following are presented for the three cases with aspect ratio of 1/10 the J_I results against the J_{IC} values, see Figures 6.5-7 to 6.5-9. In the legends of these figures JIC-1 is J_{IC} value for 33 cm³ H₂/kg H₂O without pre-exposure, JIC-2 is J_{IC} value for 100 cm³ H₂/kg H₂O with pre-exposure, and JIC-3 is J_{IC} value for 100 cm³ H₂/kg H₂O without pre-exposure, whereas 90 ° is crack tip location, respectively.

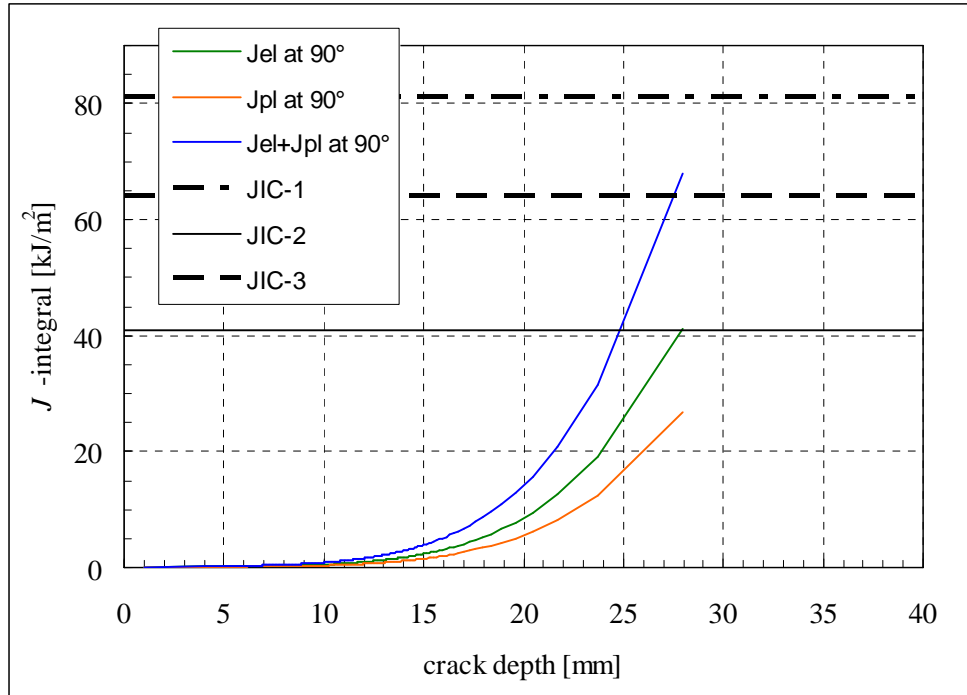


Figure 6.5-7. The J_I results against the J_{IC} values for inner axial semi-elliptical surface crack at assumed DMW; Case 10 with aspect ratio of 1/10.

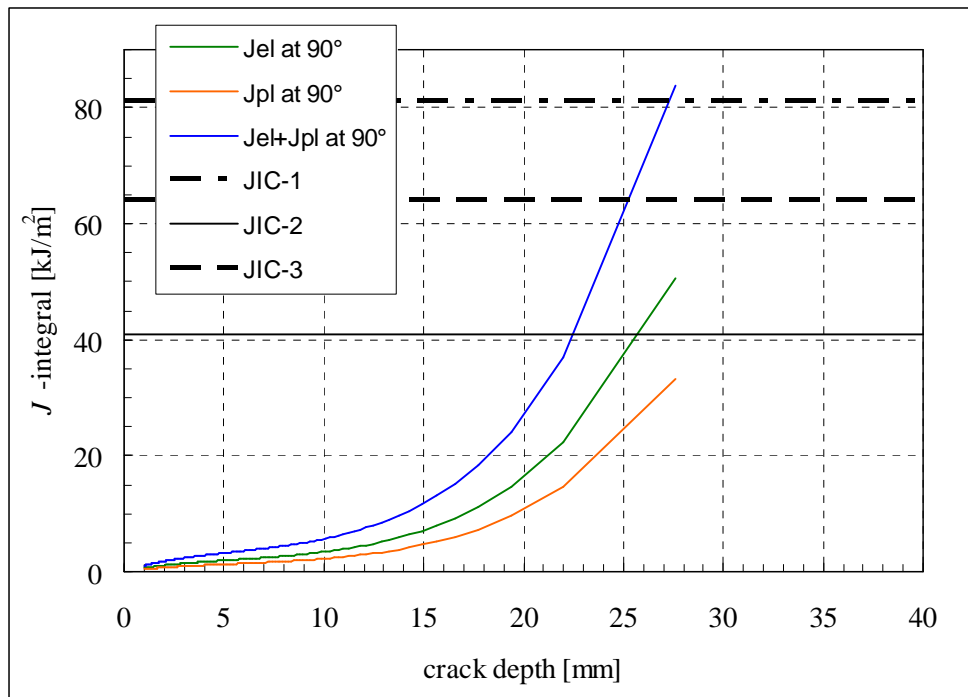


Figure 6.5-8. The J_I results against the J_{IC} values for inner axial semi-elliptical surface crack at assumed DMW; Case 11 with aspect ratio of 1/10.

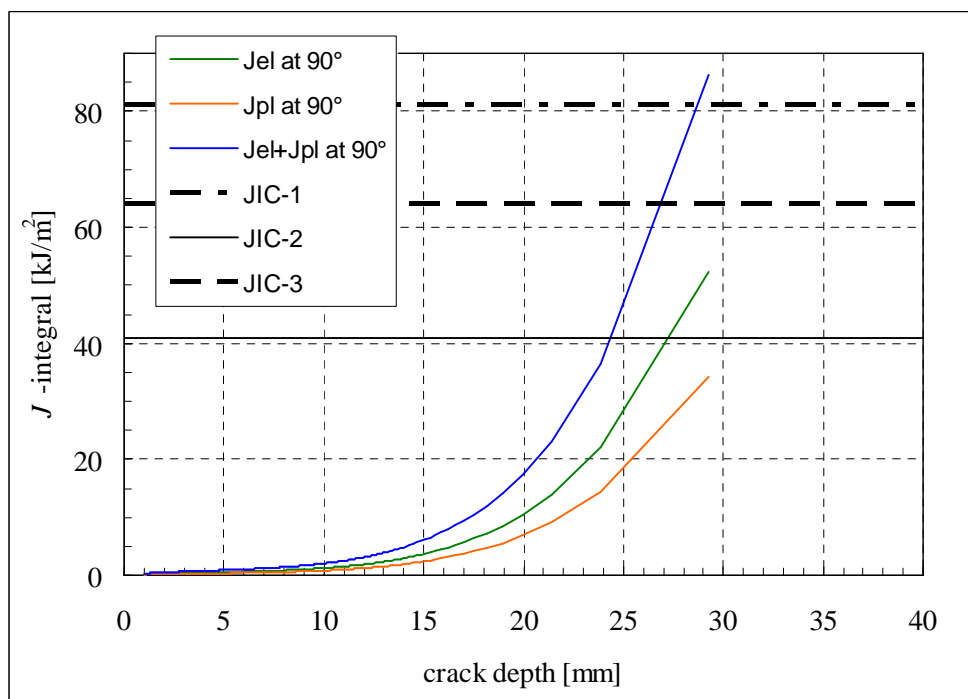


Figure 6.5-9. The J_I results against the J_{IC} values for inner axial semi-elliptical surface crack at assumed DMW; Case 12 with aspect ratio of 1/10.

In the following Table 6.5-1 are presented for analysis cases 4 to 12 those crack depths and lengths for which the crack tip J_I results match the corresponding J_{IC} values. The first three analysis cases with lower resulting J_I values, remaining below the considered J_{IC} values, were excluded from the Table 6.5-1.

Table 6.5-1. For analysis cases 4 to 12 those crack depths & lengths for which the J_I results match the corresponding J_{IC} values. Here JIC-1 is J_{IC} value for $33 \text{ cm}^3 \text{ H}_2/\text{kg H}_2\text{O}$ without pre-exposure, JIC-2 is J_{IC} value for $100 \text{ cm}^3 \text{ H}_2/\text{kg H}_2\text{O}$ with pre-exposure, and JIC-3 is J_{IC} value for $100 \text{ cm}^3 \text{ H}_2/\text{kg H}_2\text{O}$ without pre-exposure, and $1/2$ Length is half of crack length, with the fracture toughness data taken from ref. [1].

Analysis Case	Crack Depth/ $1/2$ Length [mm/mm] at JIC-2 of 41 kJ/m^2	Crack Depth/ $1/2$ Length [mm/mm] at JIC-3 of 64 kJ/m^2	Crack Depth/ $1/2$ Length [mm/mm] at JIC-1 of 81 kJ/m^2
4	29.2 / 87.6	33.6 / 100.8 (*)	36.8 / 110.4 (*)
5	29.2 / 87.6	35.0 / 105.0	39.3 / 117.9 (*)
6	29.7 / 89.1	35.0 / 105.0 (*)	38.6 / 115.8 (*)
7	26.9 / 134.5	30.8 / 154.0 (*)	33.1 / 165.5 (*)
8	25.4 / 127.0	29.3 / 146.5	32.2 / 161.0 (*)
9	26.9 / 134.5	30.2 / 151.0	32.3 / 161.5
10	24.6 / 246.0	27.3 / 273.0	29.6 / 296.0 (*)
11	22.4 / 224.0	25.0 / 250.0	27.0 / 270.0
12	24.2 / 242.0	26.8 / 268.0	28.6 / 286.0

(*): In the cases coloured with orange the J_I results were extrapolated up to the outer surface at 40 mm, as VTTBESIT had stopped computation earlier because the next increment would have exceeded the wall thickness, which is not allowed.

7 Summary and conclusions

This study concerns structural integrity analyses in connection with the LTCP phenomenon, which is associated with relatively low material fracture toughness values. Especially this phenomenon concerns PWR plants because, and unlike in BWR plants, PWR environments may contain notable amounts of hydrogen.

The structural integrity analyses were performed to a DMW at a nozzle/safe-end joint resembling that in PWR plants. The considered material was Alloy 182, for which the needed fracture toughness data corresponding to LTCP conditions was obtained from the recent VTT experiments, as reported in ref. [1]. Firstly the transient temperature and stress/strain distributions through the DMW wall were computed using analytical equations and numerical temperature/stress analysis code DIFF [10]. Also WRS distributions were taken into account, here according to assumptions in the SSM Handbook [17]. In the crack sensitivity analyses the considered crack postulate was axial half-elliptic crack in the inner surface of the assumed DMW at a nozzle/safe-end joint, with covering a representative set of aspect ratios and crack depths, while the considered load cases were Shutdown and Emergency cooling transients. Then the K_I analyses were performed for these crack postulates with a fracture mechanics based analysis code VTTBESIT [18, 19, 20]. As the considered material is an austenitic alloy with relatively large strain hardening region, elastic-plastic fracture mechanics associated with assessment of ductile fracture was applied. As for the considered limiting criterion, in the present analyses it was the crack tip value of J -integral reaching the corresponding fracture toughness, J_{IC} .

The LTCP conditions which are associated with prevailing temperature of 55 °C do not occur often in actual PWR environments, nor do they last long. As a result of the prior screening it was deduced that the LTCP conditions may take place mainly during the load transients Shutdown and Emergency cooling. This is why only these two load transients were taken into account in the performed crack sensitivity analyses. The former of these load transients occurs yearly a few times, and stays within a temperature region of some degrees centred around 55 °C for approximately ten minutes. Whereas the Emergency cooling is an exceptional load transient corresponding to some types of malfunctions or accidents. Thus this transient occurs typically from a few to less than ten times during operational lifetime [8, 9]. Moreover, during it the LTCP conditions take place only for some tens of seconds, due to rapid altering of fluid temperature. Why Start-up, which is the obvious counterpart for Shutdown, was excluded from the considered load transients, is that when during it the LTCP conditions are reached, the corresponding pressure is much lower than that for Shutdown, thus making it much less severe from the structural integrity viewpoint.

The procedures applied here to compute elastic and plastic J -integral are to some extent approximate. More accurate J -integral values would have been obtained with three dimensional finite element method (FEM) based analyses. However, this latter option was beyond the scope of this study, due to elastic-plastic fracture mechanics FEM analyses being computationally laborious to perform. All in all the applied fracture mechanics procedures are well enough accurate for the present analyses, actually they mostly correspond to those in the advanced and continuously updated fitness-for-service handbook R6 Method, Rev. 4 [12].

In some cases concerning the presented J_I results it was necessary to extrapolate them up to the outer surface at 40 mm, as VTTBESIT had stopped computation earlier because the next increment would have exceeded the wall thickness, which is not allowed. However, in these cases the increase of J_I values had already adopted during several earlier increments a linear slope, and most likely the next point exceeding the wall thickness would have fallen on the continuation of this slope as well. Thus it is deemed that the performed linear J_I result extrapolations are appropriate and accurate enough.

For all analysis cases exceeding one or several of the considered J_{IC} values associated with the LTCP, the corresponding crack sizes are relatively large, e.g. in the depth direction from 52 to 98 % of the wall thickness. Growing cracks are most likely detected in the inspections with non-destructive testing (NDT) techniques before they reach these large sizes. According to present analysis results for narrow cracks with aspect ratio of 1/1 the crack tip J_I values stay below the corresponding J_{IC} values, even with extrapolation.

Assessment of crack growth rates was not covered in this study. This was mainly caused by not having at the time available applicable data relating the increase in J_I values of a growing crack to time dependent degradation mechanism. Often for welds of Alloy 182 the assumed degradation mechanism is stress corrosion cracking (SCC). Then a commonly applied approach to compute the crack growth rates is to use the so called rate equation, where the time derivative of crack depth propagation is expressed as related to K_I together with some experimentally assessed material and environment specific parameters. So one option could be to compute the crack growth rate this way, and then consider possible crack arrest at each time increment by comparing the crack tip and/or maximum J_I value to the corresponding fracture resistance value, obtained from the associated fracture resistance curve. Also, according to experimental data the fracture resistance values increase as a function of crack growth. This mentioned computation approach provides some confusion, though, as for the LTCP conditions there would be one value for J_{IC} , and then another for the normal operation, and somehow also J_{IC} values should be obtained for all other typically anticipated/experienced plant conditions and load transients. Moreover, typically crack growth rate equations do not even include fracture toughness, and thus e.g. in computations cracks propagate in the material considered as susceptible to SCC for as long as the K_I values caused by loading exceed the threshold values, which often are very low. Thus it appears that more data collecting and computation approach development should be provided before proceeding to crack growth rate computations. Relatively rapid crack growth occurs during the LTCP conditions, so even though the durations for these conditions to prevail are quite short, at least to examine/ensure this matter it would be worthwhile to develop some robust analytical approach allowing to carry out accurate enough crack growth rate computations.

Finally, in the following are some suggestions for possible further research. Concerning computational examinations, the growth of crack postulates that extend from the weld region through the material interfaces and HAZs to the base material sides could be attempted to simulate with three dimensional FEM analyses. This would necessitate collaboration with experimental research, e.g. to obtain data concerning the changing of the material properties within the HAZ region from those of the weld material to those of the base material, respectively. These material property value changes that can take place within relatively short distances when moving through the material regions necessitate the preparation of markedly dense FEM meshes. Also needed are more detailed experimental data of crack growth in DMWs. The WRS distributions in fitness-for-service handbooks/procedures, such as those applied here,

are more or less conservative. More realistic WRSs could be obtained with FEM simulations. More useful, however, could be to develop a robust analytical approach to assess the crack growth rate under the LTCP conditions. This could also be carried out by further developing and/or extending an existing approach, for which possible candidates would be looked for from the available literature worldwide. All/any provided computational developments would be validated against experimental data, and possibly against other applicable computational analysis results.

References

1. Ahonen, M. Effect of Hydrogenated Low Temperature Water on Fracture Toughness of Nickel Based Weld Metals. Research Report No. VTT-R-00474-10, Technical Research Centre of Finland (VTT), January 2010, Espoo, Finland. 45 p.
2. Ahonen, M. Ympäristön ja muodonmuutosnopeuden vaikutus austeniittisten materiaalien murtumisvastuskäyttäytymiseen. Research Report VTT-R-06172-08, Technical Research Centre of Finland (VTT), Espoo, Finland, October 2008. 64 p. (Master's Thesis in Finnish)
3. Nuclear Power Plant Unit Olkiluoto 3. Brochure Document, Teollisuuden Voima Oyj (TVO), Olkiluoto, Finland, 2008. 62 p.
4. Miteva, R., Taylor, N., G. General Review of Dissimilar Metal Welds in Piping Systems of Pressurised Water Reactors, Including WWER Designs. Report EUR 22469 EN, European Commission, Joint Research Centre (JRC), Petten, Netherlands, 2006. 62 p.
5. Pilot studies on management of ageing of nuclear power plant components - Results of Phase I. Technical Document IAEA-TECDOC-670, Vienna, Austria, October 1992. 103 p.
6. EricksonKirk, M. et al. Technical Basis for Revision of the Pressurized Thermal Shock (PTS) Screening Limit in the PTS Rule (10 CFR 50.61) - Summary Report. Report No. NUREG-1806, Vol. 1, U.S. Nuclear Regulatory Commission (USNRC), Washington DC, August 2007. 339 p.
7. RELAP5-3D CODE MANUAL VOLUME I: CODE STRUCTURE, SYSTEM MODELS, AND SOLUTION METHODS, Revision 2.4. Idaho National Laboratory Report INEEL-EXT-98-00834, U.S., June 2005. 600 p.
8. NUCLEAR TECHNOLOGY REVIEW 2010. International Atomic Energy Agency (IAEA), Austria, September 2010. 167 p.
9. Lydell, B., Riznic, J. OPDE - The International Pipe Failure Data Exchange Project. Nuclear Engineering and Design, Vol. 238, pp. 2115-2123, 2008.
10. Raiko, H. et al. Paineistetun termoshokin analysointiohjelma DIFF. Valtion teknillinen tutkimuskeskus (VTT), Valmistustekniikka, työraportti LUJA-1/94. 16.11.1994. 27 p. (in Finnish).
11. Ylinen, A. Kimmo- ja lujuusoppi, parts I – II, 2nd Edition. WSOY, Porvoo, Finland, 1969. 1010 p. (in Finnish).
12. R6 Method; Assessment of the Integrity of Structures containing Defects, Revision 4. 2004 update of 2001 edition. British Energy (BE).
13. ASME Boiler and Pressure Vessel Code, Section II. 2005 Update of 2004 Edition.

14. Ainsworth, R., A. The Assessment of Defects in Structures of Strain Hardening Material. Engineering Fracture Mechanics, Vol. 19, No.4, pp. 633-642, 1984.
15. Ainsworth, R., A. Analysis methods for the practical application of fracture mechanics. 7th International Conference on Modern Practice in Stress and Vibration Analysis, Journal of Physics: Conference Series 181 (2009) 012003.
16. Section XI Task Group for Piping Flaw Evaluation, ASME Code. Evaluation of Flaws in Austenitic Steel Piping. Journal of Pressure Vessel Technology, Vol. 108, 1986. Pp. 352-366.
17. Dillström, P. et al. 2008. A Combined Deterministic and Probabilistic Procedure for Safety Assessment of Components with Cracks – Handbook. SSM Research Report 2008:01, Swedish Radiation Safety Authority (Strålsäkerhetsmyndigheten, SSM). Stockholm, Sweden, 2008. 27+196 p.
18. Varfolomeyev, I. et al. BESIF 1.0: Stress Intensity Factors for Surface Cracks under 2D Stress Gradients. IWM-Report T 14/96, Fraunhofer-Institut für Werkstoffmechanik (IWM), July 1996. 42 p.
19. Busch, M. et al. K_I -Factors and Polynomial Influence Functions for Axial and Circumferential Surface Cracks in Cylinders. IWM-Report T 18/94, Fraunhofer-Institut für Werkstoffmechanik (IWM), October 1994. 41 p.
20. Busch, M. et al. Polynomial Influence Functions for Surface Cracks in Pressure Vessel Components. IWM-Report Z 11/95, Fraunhofer-Institut für Werkstoffmechanik (IWM), January 1995. 88 p.
21. ASME Boiler and Pressure Vessel Code, Section XI. 2009 Update of 2007 Edition.